Electronic supplementary information (ESI)

Remote conformational responses to enantiomeric excess in carboxylate-binding dynamic foldamers

Natasha Eccles,[1,2] Bryden A. F. Le Bailly,[1,3] Flavio della Sala,[1,2] Iñigo J. Vitórica-Yrezábal,[1] Jonathan Clayden[3,]* and Simon J. Webb[1,2,]*

1. *School of Chemistry, University of Manchester, Oxford Road, Manchester M13 9PL, United Kingdom.*

2. *Manchester Institute of Biotechnology, University of Manchester, 131 Princess St, Manchester M1 7DN, United Kingdom. E-mail: S.Webb@manchester.ac.uk; Tel: +44 161 306 4524.*

3. *School of Chemistry, University of Bristol, Cantock's Close, Bristol BS8 1TS, UK. E-mail: j.clayden@bristol.ac.uk*

*. Email: S.Webb@manchester.ac.uk, j.clayden@bristol.ac.uk

TABLE OF CONTENTS

1. Chemical synthesis: instruments

All ^{1}H and ^{13}C nuclear magnetic resonance (NMR) spectra were obtained using Bruker AVANCE 400 or 500 spectrometers. Chemical shifts are quoted in parts per million (ppm) and coupling constants (J) are quoted in Hz to the nearest 0.5 Hz. ^{1}H NMR shifts were referenced to the solvent peak ($CDCl_3$ 7.27; CD_3OD 3.31; DMSO-d_6 2.50; CD_3CN 1.94, THF-d_8 1.73, D_2O 4.79 ppm) and ^{13}C NMR were referenced to the carbon resonance of the solvent ($CDCl_3$ 77.0; CD_3OD 49.0; DMSO-d_6 39.5; CD_3CN 118.2, THF-d_8 67.2 ppm). For spectra from the Bruker AVANCE 400 NMR spectrometer, the FID resolution is 0.24 Hz, and the digital resolution in processed spectra is 0.12 Hz. Multiplicities are denoted as s (singlet), d (doublet), t (triplet), q (quartet), m (multiplet) or denoted as br (broad), or some combination of these, where appropriate. Assignments were made using 2D ^{1}H-COSY, TOCSY and HMQC experiments. The anisochronicity, in parts per billion (ppb), of AB systems arising from the germinal ^{1}H nuclei of the $GlyNH_2$ diastereotopic NMR probe was given by $u_0\,\Delta\delta = [(f_1 - f_3)^2 - J_{AB}^2]^{1/2} = [(f_2 - f_4)^2 - J_{AB}^2]^{1/2} = [(f_1 - f_4)\,(f_2 - f_3)]^{1/2}$ where $f_{1,2,3,4}$ are the observed resonant frequencies in order of the four lines comprising the AB multiplet, J_{AB} is the coupling constant and u_0 is the spectrometer frequency.

Optical rotation ($[\alpha]_D^T$) measurements were taken on a AA-100 polarimeter at 20 °C using a cell with a pathlength of 0.25 dm. The solvent and concentration are stated with individual readings. Melting points (mp) were determined on a GallenKamp apparatus and are uncorrected. Infra-red spectra (IR) were recorded on an ATi Perkin Elmer Spectrum RX1 FT-IR. Only absorption maxima (v_{max}) of interest are reported and quoted in wavenumbers (cm^{-1}). Low- and high-resolution mass spectra were recorded by staff at the University of Manchester. Electrospray (ES) spectra were recorded on a Waters Platform II. High-resolution mass spectra (HRMS) were recorded on a Thermo Finnigan MAT95XP and are accurate to ±0.001 Da. HPLC analyses were performed on an Agilent 1100 Series instrument equipped with a Chiralpak® AD-H (0.46 × 25 cm) column.

2. Chemical synthesis: materials

2.1 Abbreviations

EDC·HCl: 1-ethyl-3-(3-dimethylaminopropyl)carbodiimide, BQPA: *N,N*-bis[2-quinolyl]methyl-*N*-[2-pyridyl]methylamine, DMAP: 4-(dimethylamino)pyridine, TFA: trifluoroacetic acid, IPA: *iso*propyl alcohol, Hex: hexane, MeCN: acetonitrile, MeOH: methanol, Quin: quinolone, THF: tetrahydrofuran.

2.2 Structures of anhydrides
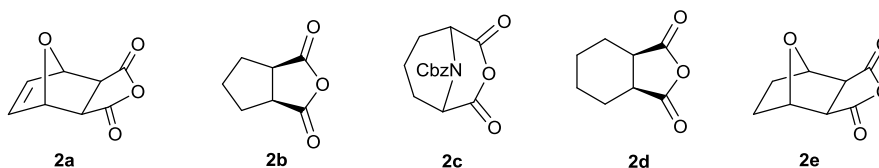
2.3 Materials

All reactions were carried out in oven-dried glassware under an atmosphere of nitrogen using standard anhydrous techniques. All reagents were obtained from commercially available sources and used without further purification, or where indicated prepared internally. Anhydrous THF was obtained by drying with activated 4Å molecular sieves. Reactions performed at −20 °C were performed in a freezer at this temperature. All products were dried on a rotary evaporator followed by connection to a high vacuum system to remove any residual solvent. Flash chromatography was performed on silica gel (Merck 60H, 40-60 nm, 230–300 mesh). Analytical thin layer chromatography (TLC) was performed on Macherey Nagel alugram SIL G/UV254 and were visualised by UV (254 nm), ninhydrin or potassium permanganate dyes where appropriate. Anhydrides **2a**, **2b** and **2d** were obtained from Sigma Aldrich UK. The foldamer (BQPA)Aib$_4$GlyNH$_2$ **1** was synthesised as reported previously.[1] The quinoline based organocatalyst **4** was prepared from 9-amino-(9-deoxy)-*epi*-quinine (prepared by a method reported by Cavaleiro and co-workers[2]) by the method of Song and co-workers.[3] (3a*R*,7a*S*)-Hexahydro-4,7-epoxyisobenzofuran-1,3-dione **2e** was synthesised following literature procedures and gave satisfactory spectroscopic data.[4]

3. Synthetic procedures

3.1 Zn(1).2ClO₄
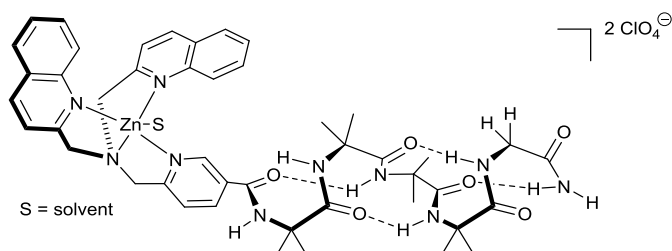
Compound **1** (550 mg, 0.63 mmol) was dissolved in MeOH (18.4 mL). $Zn(ClO_4)_2.6H_2O$ (157 mg, 0.63 mmol) was added dropwise as a solution in MeOH (9.2 mL) and the resulting solution was stirred at r.t. for 10 min. Et_2O (10 mL) was added dropwise until saturation and the heterogeneous mixture was cooled to 0 °C. The remaining Et_2O (46.7 mL) was added and the suspension was stirred for 1 h. The suspension was filtered to give the title compound as a pale-yellow solid (600 mg, 85%). **¹H NMR** (400 MHz, CD_3CN): δ_H 9.02 (1H, br s, PyCH), 8.61 (2H, d, J = 8.6, 2 × QuinCH), 8.59 (2H, d, J = 9.0, 2 × QuinCH), 8.47 (1H, dd, J = 8.2, 1.9, PyCH), 8.11 (2H, d, J = 8.1, 2 × QuinCH), 8.03 (2H, app. t, J = 7.9, 2 × QuinCH), 7.78 (2H, app. t, J = 7.6, 2 × QuinCH), 7.75–7.65 (4H, m, 2 × NH, PyH, <u>NH</u>CH₂), 7.61 (2H, d, J = 8.5, 2 × QuinCH), 7.55 (1H, br s, NH), 7.40 (1H, br s, NH), 7.30 (1H, br s, NH), 6.30 (1H, br s, NH), 4.69 (2H, d, J = 17.5, QuinCH₂, H^A of AB system), 4.59 (2H, d, J = 17.5, QuinCH₂, H^B of AB system), 4.58 (2H, s, PyCH₂), 3.91 (2H, d, J = 5.1, <u>CH₂</u>NH), 1.51 (6H, s, 2 × CH₃), 1.39 (6H, s, 2 × CH₃), 1.36 (6H, s, 2 × CH₃), 1.34 (6H, s, 2 × CH₃) ppm. **¹³C NMR** (101 MHz, CD_3CN) δ_C 177.2 (CO), 176.94 (CO), 176.92 (CO), 176.7 (CO), 175.3 (CO), 165.3 (CO-Py), 160.0 (QuinC), 158.6 (PyC), 148.1 (PyCH), 145.8 (QuinC), 143.1 (QuinCH), 141.4 (PyCH), 133.8 (QuinCH), 132.4 (PyC), 130.0 (QuinC), 129.9 (QuinCH), 129.3 (QuinCH), 126.7 (QuinCH), 125.5 (PyCH), 122.6 (QuinCH), 60.4 (CH₂-Quin), 59.1 (CH₂-Py), 58.6 ($^\alpha$C), 57.6 ($^\alpha$C), 57.53 ($^\alpha$C), 57.51 ($^\alpha$C), 43.9 (CH₂-NH), 25.5 (CH₃), 25.2 (CH₃), 25.01 (CH₃), 25.00 (CH₃). **m.p.:** >266 °C (decomp.). **MS** (ESI, MeOH): m/z 447 ($[Zn^{64}(BQPAAib_4GlyNH_2)]^{2+}$, 20%), 449 ($[Zn^{68}(BQPAAib_4GlyNH_2)]^{2+}$, 100%), 893 ($[Zn^{64}(BQPAAib_4GlyNH_2)-H]^+$, 20%, 894 ($[Zn^{65}(BQPAAib_4GlyNH_2)-H]^+$, 5%), 895 ($[Zn^{66}(BQPAAib_4GlyNH_2)-H]^+$, 10%). **IR** (ATIR, λ_{max}): br 3310, 2987, 2943, 1651, 1603, 1531, 1459, 1435, 1386, 1087 cm⁻¹. **UV/Vis:** λ_{max} 201, 233 nm.

3.2 Anhydride 2c
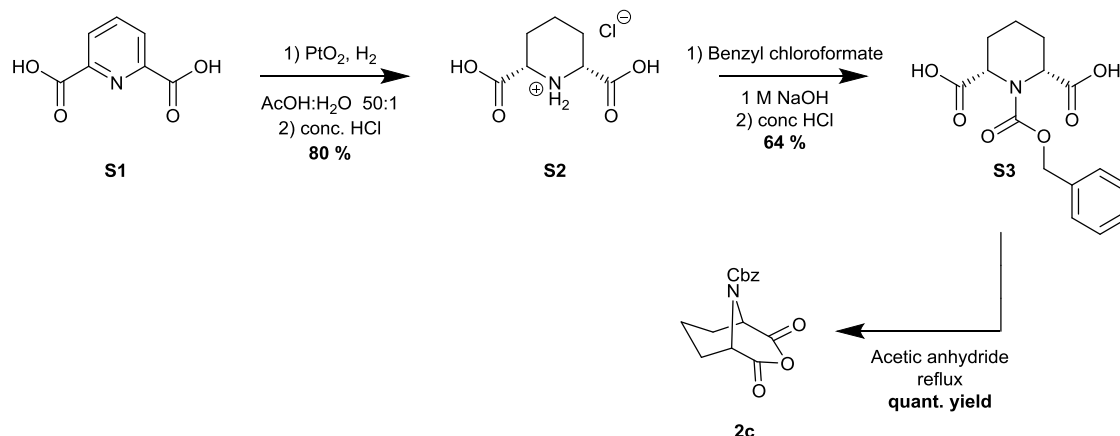
Scheme S1: Scheme showing the synthesis of *meso*-anhydride **2c**.

3.2.1 Synthesis of *meso*-piperidine-2,6-dicarboxylic acid (S2)
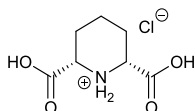
Compound **S2** was synthesised by following the procedure of Chrystal *et al.*[5] 2,6-Pyridinedicarboxylic acid **S1** (1.50 g, 8.97 mmol) was dissolved in glacial acetic acid (50 mL) and H_2O (1 mL). PtO_2 (150 mg) was added in one portion and the suspension was vigorously stirred under H_2 for 35 h. The reaction mixture was filtered through a pad of Celite® and the filtrate was acidified with conc. HCl until precipitation occurred. The precipitate was collected by vacuum filtration and recrystallised from H_2O to give **S2** a colourless solid (1.23 g, 80%). **¹H NMR** (400 MHz, D_2O): δ_H 4.02–3.91 (2H, m, 2 × $^\alpha$CH), 2.34–2.26 (2H, m, 2 × CH of CH_2), 2.07–2.01 (1H, m, CH of CH_2), 1.73–1.58 (3H, m, 3 × CH of CH_2) ppm. **¹³C NMR** (101 MHz, D_2O): δ_C 171.1 (CO), 56.9 (CH), 25.0 (CH_2), 21.8 (CH_2) ppm. **MS** (ESI⁻, MeOH): 172.0 (100%, [M–H]⁺). **HRMS** (ESI⁺, MeOH): *m/z* calcd. for $C_7H_{11}NO_4$ ([M+H]⁺) = 174.0761, found 174.0762. **IR** (ATIR, ν_{max}): 2963, 2938, 1736, 1385 cm⁻¹.

3.2.2 Synthesis of *meso*-1-((benzyloxy)carbonyl)piperidine-2,6-dicarboxylic acid (S3)
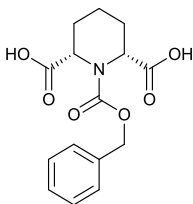
Compound **S3** was synthesised by a modification of the procedure of Chong *et al.*[6] Benzyl chloroformate (196 mg, 1.15 mmol) was added dropwise to a stirring solution of (2*S*,6*R*)-piperidine-2,6-dicarboxylic acid (100 mg, 0.57 mmol) in 1 M NaOH (1.2 mL) at 0 °C. The reaction mixture was warmed to r.t. and stirred for 24 h. The reaction mixture was extracted with diethyl ether (2 × 4 mL) to remove the excess benzyl chloroformate. The aqueous layer was acidified (conc. HCl) and the product was precipitated out. This was collected by filtration to give the title compound as a white crystalline solid (140 mg, 64%).**^{1}H NMR** (400 MHz, DMSO-d_6): δ_H 7.38–7.30 (5H, m, ArH), 5.11 (2H, s, CH$_2$), 4.64 (2H, dd, *J* = 6.2, 2.1, 2 × CH), 2.01–1.98 (2H, m, CH$_2$), 1.72–1.62 (2H, m, CH$_2$), 1.54–1.43 (2H, m, CH$_2$) ppm. **^{13}C NMR** (101 MHz, DMSO-d_6): δ_C 173.4 (CO), 155.5 (CO), 136.5 (ArC), 128.3 (ArCH), 127.7 (ArCH), 127.2 (ArCH), 66.7 (CH$_2$Ar), 52.9 (CH), 25.4 (CH$_2$), 16.3 (CH$_2$) ppm. **MS** (ESI⁻, MeOH): 306.1 (100%, [M–H]⁺). **HRMS** (ESI⁻, MeOH): *m/z* calcd. For C$_{15}$H$_{16}$O$_6$N ([M–H]⁺) = 306.0972, found 306.0979. **IR** (ATIR, v$_{max}$): 2917, 1709, 1616, 1388, 1341 cm⁻¹.

3.2.3 Synthesis of benzyl *meso*-2,4-dioxo-3-oxa-9-azabicyclo[3.3.1]nonane-9-carboxylate (2c)
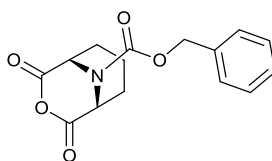
Compound **2c** was synthesised by a modification of the procedure of Babine *et al.*[7] *meso*-1-((Benzyloxy)carbonyl)piperidine-2,6-dicarboxylic acid (200 mg) was dissolved in acetic anhydride (2 mL) under N$_2$ and was refluxed for 1 h at 70 °C. The reaction mixture was cooled and purified by co-evaporation with toluene (5 × 3 mL) to remove all traces of acetic anhydride. The anhydride was obtained as a colourless oil after drying under vacuum (quant yield). This oil was used immediately without characterisation.

3.3 Desymmetrisation of *meso*-anhydrides

3.3.1 General procedure 1: methanolytic desymmetrisation of *meso*-anhydrides, catalysed by 4.
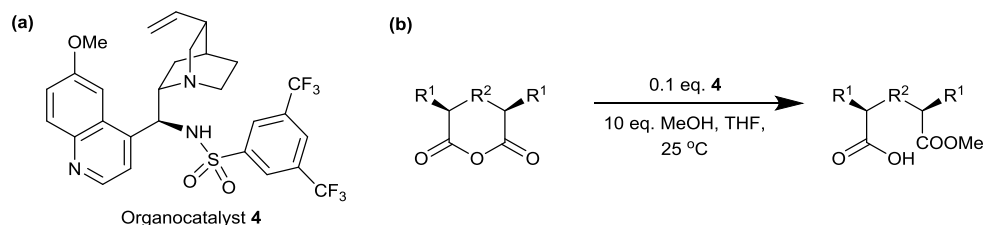
Scheme S2: (a) Organocatalyst **4 (b)** General scheme showing desymmetrisation of *meso*-anhydrides.

The requisite *meso*-anhydride (0.50 mmol) and the chiral catalyst **4** (0.1 eq.) were dissolved in anhydrous THF (5 mL) under argon at r.t.. Anhydrous MeOH (5 mmol) was added dropwise and the solution was stirred until TLC/NMR spectroscopy indicated completion of the reaction. The catalyst was quenched by the addition of HCl (1 M, 5 mL) and was extracted with EtOAc (2 × 50 mL). The organic layers were combined, dried over MgSO$_4$ and concentrated to give the product monoester. In some cases, purification was required (specified for each individual compound).

3.3.2 General procedure 2: conversion of monoesters to diastereoisomeric amides by reaction with (*R*)-naphthylethylamine
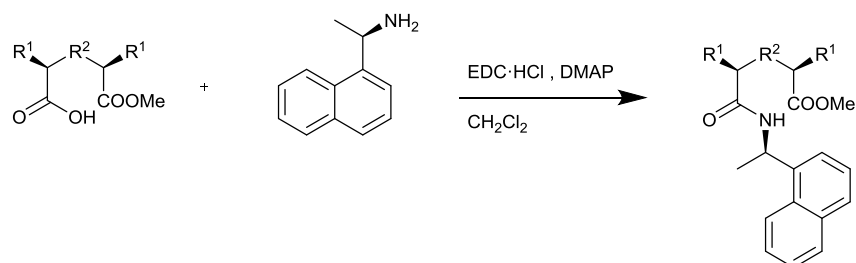
Scheme S3: General scheme showing coupling of monoesters to (*R*)-naphthylethylamine

The requisite chiral acid (1 eq.), and EDC·HCl (1.2 eq.) were dissolved in anhydrous CH$_2$Cl$_2$ (0.05 mmol.mL^{-1}) at 0 °C and was stirred for 20 mins. (*R*)-Naphthylethylamine (1.2 eq.) and DMAP (0.05 eq.) were added dropwise as a solution in anhydrous CH$_2$Cl$_2$ and the reaction mixture was warmed to r.t. and stirred overnight. The reaction mixture was washed with 1 M HCl and sat. NaHCO$_3$, dried over MgSO$_4$ and concentrated to give the diastereoisomeric mixture. The enantiomeric excesses (*e.e.*) of the monoesters were determined by HPLC analysis of the diastereoisomeric mixtures (see Section S5.1) or by ^{1}H NMR spectroscopic analysis (see Section S5.2).

3.3.3 (1*S*,2*R*,3*S*,4*R*)-3-(Methoxycarbonyl)-7-oxabicyclo[2.2.1]hept-5-ene-2-carboxylic acid (3a)
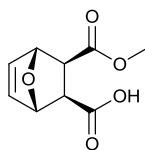
Following general procedure **1**, the monoester was obtained as a colourless crystalline solid (97 mg, 98%). A 93% *e.e.* was obtained; this was determined by the conversion of the enantiomers into diastereoisomers following general procedure **2**. For HPLC analysis, the diastereoisomeric mixture was dissolved in a mixture of Hex:IPA (1:1, 1 mg mL^{-1}). The sample was separated using a Chiralpak® AD-H column (0.46 × 25 cm, 1 mL/min, 80:20 Hex:IPA, 210 nm) t_1 = 9.463, t_2 = 12.450 min.

R$_f$ (EtOAc:Hex 1:1) 0.5. **m.p.:** 110–111 $^{\circ}$C. **[α]$_D$$^{29.4}$** = +1.38 (C = 1.18, CHCl$_3$).**^{1}H NMR** (400 MHz, CDCl$_3$): δ$_H$ 6.49–6.45 (2H, m, 2 × C<u>H</u>=CH), 5.25 (1H, app. t, *J* = 1.3, CH-O), 5.21 (1H, app. t, *J* = 1.3, CH-O), 3.70 (3H, s, OCH$_3$), 2.82–2.77 (2H, m, 2 × CH) ppm. **^{13}C NMR** (101 MHz, CDCl$_3$): δ$_C$ 177.5 (CO), 171.8 (CO), 136.9 (C=C) 136.5 (C=C), 80.7 (CH-O), 80.4 (CH-O), 52.5 (OCH$_3$), 47.4 (CH), 47.0 (CH) ppm. Data is consistent with that reported in the literature and the absolute configuration was established by comparing the optical rotation with literature data.[8]

3.3.4 (1*S*,2*R*)-2-Methoxycarbonyl-cyclopentane-1-carboxylic acid (3b)

Following general procedure **1,** the *hemi*-ester was obtained as a colourless oil (quant. yield). A 95 ± 1% *e.e.* was obtained; this was determined by the conversion of the enantiomers into diastereoisomers following general procedure **2**. The ^{1}H NMR spectra of the diastereoisomers was acquired at 20 °C in CDCl$_3$.

[α]$_D$$^{19.4}$ = –2.0 (C = 0.5, MeOH). *R*$_f$ (Hex:EtOAc 3:1) 0.17. **^{1}H NMR** (400 MHz, CDCl$_3$): δ$_H$ 3.65 (3H, s, CH$_3$), 3.10–3.06 (2H, m, 2 × CH), 1.99–1.80 (5H, m, 2 × CH$_2$, CH of CH$_2$), 1.64 (1H, m, CH of CH$_2$) ppm. **^{13}C NMR** (101 MHz, CDCl$_3$): δ$_C$ 180.0 (CO), 174.4 (CO), 51.8 (CH$_3$), 46.8 (CH), 46.7 (CH), 28.7 (2 × CH$_2$), 23.8 (CH$_2$) ppm. Data is consistent with that reported in the literature and the absolute configuration was established by comparing the optical rotation with literature data.[9]
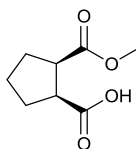
3.3.5 *cis*-1-((Benzyloxy)carbonyl)-6-(methoxycarbonyl)piperidine-2-carboxylic acid (3c)
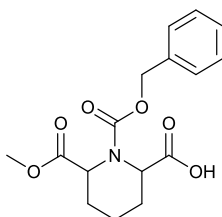
The *meso*-anhydride (144.5 mg, 0.50 mmol) and organocatalyst **4** (329 mg, 0.55 mmol) were dissolved in anhydrous THF (22.4 mL) under argon at –20 °C. Anhydrous MeOH (22.7 µL, 0.50 mmol) was added dropwise and the solution was stirred at –20 °C until NMR spectroscopy indicated the completion of reaction. The catalyst was quenched by the addition of HCl (1 M, 5 mL) and was extracted with EtOAc (50 mL × 2). The organic layers were combined, dried over MgSO$_4$ and concentrated to give the chiral monoester that was purified by column chromatography (SiO$_2$, neat EtOAc). The title compound was obtained as a colourless oil (144 mg, 90%). A 96 ± 1 % *e.e.* was obtained; this was determined by HPLC analysis of the monoester. The monoester was dissolved in a mixture of Hex:IPA (1:1, 1 mg mL^{-1}) and the sample was separated using a Chiralpak® AD-H column (0.46 × 25 cm, Hex:IPA 95:5, 1.2 mL min^{-1}, t_1 = 34.065, t_2 = 39.872 min).

$[\alpha]_D^{21.4}$ = –4.5 (C = 5.4 MeOH). **^{1}H NMR** (400 MHz, CDCl$_3$): δ_H **Major rotamer:** 7.38–7.28 (5H, m, 5 × ArH), 5.30–5.09 (2H, m, CH$_2$Ar), 4.79–4.65 (2H, m, 2 × CH), 3.85 (3H, s, OCH$_3$), 2.36–2.05 (2H, m, CH$_2$), 2.01–1.69 (2H, m, CH$_2$), 1.69–1.31 (2H, m, CH$_2$) ppm. **Minor rotamer:** 3.67 (3H, s, OCH$_3$) all other peaks overlap with the major rotamer. **^{13}C NMR** (CDCl$_3$, 101 MHz): δ_C **Major rotamer:** 177.8 (CO), 173.9 (CO), 155.9 (CO), 135.4 (ArC), 128.6 (2 × ArCH), 128.2 (ArCH), 128.1 (ArCH), 128.0 (ArCH), 68.6 (CH$_2$), 55.6 (CH), 53.9 (OCH$_3$), 53.6 (CH), 26.6 (CH$_2$), 25.88 (CH$_2$), 16.8 (CH$_2$) ppm. **Minor rotamer:** 175.3 (CO), 173.0 (CO), 156.4 (CO), 135.7 (ArC), 128.5 (ArCH), 128.3 (2 × ArCH), 69.8 (CH$_2$), 54.1 (CH), 54.0 (OCH$_3$), 53.1 (CH), 26.6 (CH$_2$), 25.85 (CH$_2$), 16.1 (CH$_2$) ppm. All other peaks overlap with the major isomer. **MS** (ESI$^-$, MeOH): 320.2 (100%, [M–H]$^+$). **HRMS** (ESI$^+$, MeOH): *m/z* calcd. for C$_{12}$H$_{19}$NO$_6$Na ([M+H]$^+$) = 322.1285, found 322.1286. **IR** (ATIR, ν_{max}): 2952, 1736, 1698, 1326, 1079 cm^{-1}.

3.3.6 (1*S*,2*R*)-2-(Methoxycarbonyl)cyclohexane-1-carboxylic acid (3d)
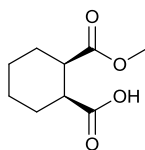
Following general procedure **1,** the monoester was obtained as a colourless oil (quant. yield). A >98% *e.e.* was obtained; this was determined by the conversion of the enantiomers into diastereoisomers following general procedure **2**. For HPLC analysis, the diastereoisomeric mixture was dissolved in a mixture of Hex:IPA (1:1, 1 mg/mL). The sample was separated using a Chiralpak® AD-H column (0.46 × 25 cm, Hex:EtOH:TFA 98:2:0.1), 1.2 mL min^{-1}, 210 nm, t_1 = 16.162, t_2 = 17.775 min.

$[\alpha]_D^{19.4}$ = +3.2 (C = 0.5, MeOH). R_f (Hex:EtOAc 3:1) 0.19. **^{1}H NMR** (500 MHz, CDCl$_3$): δ_H 3.67 (3H, s, OCH$_3$), 2.84 (2H, br s, 2 × CH), 2.03–1.98 (2H, m, CH$_2$), 1.83–1.72 (2H, m, CH$_2$), 1.58–1.34 (4H, m, 2 × CH$_2$) ppm. **^{13}C NMR** (125 MHz, CDCl$_3$): δ_C 170.8 (CO), 174.0 (CO), 51.7 (CH$_3$), 42.5 (CH), 42.3 (CH), 26.2 (CH$_2$), 25.9 (CH$_2$), 23.7 (CH$_2$), 23.6 (CH$_2$) ppm. Data is consistent with that reported in the literature,[10] and the absolute configuration was established by comparing the optical rotation with literature data.[11]

3.3.7 (1*S*,2*R*,3*S*,4*R*)-3-(Methoxycarbonyl)-7-oxabicyclo[2.2.1]heptane-2-carboxylic acid (3e)
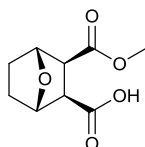
Following general procedure **1**, the *hemi*-ester was obtained as colourless crystalline solid (98 mg, 98%). A 91% *e.e.* was obtained; this was determined by the conversion of the enantiomers into diastereoisomers following general procedure **2**. ^{1}H NMR spectra of the diastereoisomers was acquired at 20 °C in CDCl$_3$.

$[\alpha]_D^{20.1}$ = +5.5 (C = 1, MeOH). **^{1}H NMR** (400 MHz, CDCl$_3$): δ_H 4.83–4.80 (2H, m, 2 × CH), 3.58 (3H, s, CH$_3$), 2.95–2.89 (2H, m, 2 × CH), 1.74–1.73 (2H, m, 2 × CH from CH$_2$), 1.47–1.45 (2H, m, 2 × CH from CH$_2$) ppm. **^{13}C NMR** (101 MHz, CDCl$_3$): δ_C 173.6 (CO), 172.3 (CO), 78.7 (CH), 78.5 (CH), 52.5 (CH), 51.9 (OCH$_3$), 49.9 (CH) 28.9 (CH$_2$), 28.8 (CH$_2$) ppm. Data is consistent with that reported in the literature[3] and the absolute configuration was established by comparing the optical rotation with literature data.[9]

4. Optimisation of organocatalysis conditions

4.1   Reaction condition optimisation for the enantioselective methanolysis of *meso*-cyclic anhydride 2a using organocatalyst 4

The desymmetrisation of anhydride **2a** with catalyst **4** was initially tested in methanol (Table S1, Entry 2). Despite the presence of the catalyst (10 mol%), a low *e.e.* of 17% was obtained, possibly due to the protic nature of methanol and its antagonism with the chiral catalyst. The desymmetrisation of **2a** in tetrahydrofuran provided the best enantioselectivity with an *e.e.* of 96% being obtained (Table S1, Entry 4 and Section 5.1.1). This was anticipated as Oh and co-workers explored solvent effects and showed that aprotic H-bonding solvents are the most effective.[10] Acetonitrile, the solvent used for monitoring conformational control of the $Zn(\mathbf{1})^{2+}$ foldamer, only delivered mild enantioselectivity (65% *e.e.*).

The enantioselectivity was deduced by conversion of the acid to diastereoisomers using (*R*)-naphthylethylamine and the product mixture was evaluated by HPLC or ^{1}H NMR spectroscopy. For example, ^{1}H NMR spectroscopic analysis of the crude mixture showed a pair of resonances that belonged to the methyl ester in each of the converted diastereoisomers (δ ~3.6 ppm). The integration of these resonances gave the ratio of diastereoisomers, which corresponds to the enantioselectivity of the desymmetrisation.

Table S1: Optimisation of the reaction conditions for the enantioselective methanolysis of *meso*-cyclic anhydride **2a** using organocatalyst **4**.
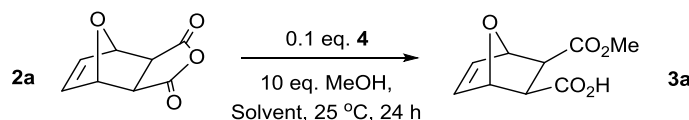
Entry	Solvent / 0.1 M[a]	Time / h	% Yield	% e.e.[b]
1	Diethyl ether	24	0	–
2	MeOH	16	51	17
3	MeCN	48	quant.	65
4	THF	28	98	96

[a] Reactions were carried out with **2a** (0.5 mmol), 10 eq. of MeOH (5 mol) and catalyst **4** (10 mol%) in an appropriate solvent (5 mL).
[b] *e.e.* was determined by HPLC on chiral stationary phase after derivatisation with (*R*)-naphthylethylamine (see Section S4.1.1).

4.1.1 HPLC traces for entries in Table S1

4.1.1.1 Table S1 – Entry 2 (MeOH, 10 mol% 4, 16 h)

Chiralpak® AD-H, 0.46 × 25 cm, 1 mL/min
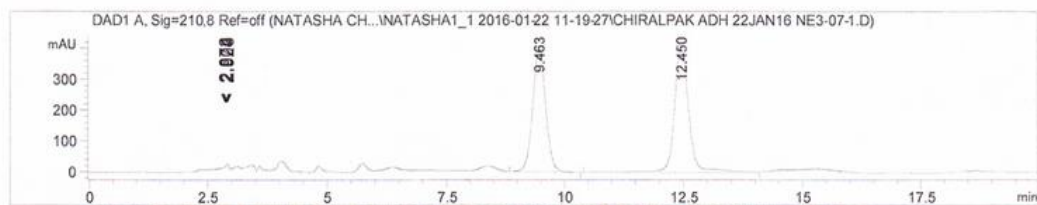
80:20 Hex:IPA, 210 nm


```
Signal 1: DAD1 A, Sig=210,8 Ref=off

Peak RetTime Type  Width     Area      Height     Area
 #    [min]        [min]   [mAU*s]     [mAU]       %
----|-------|----|-------|----------|----------|--------|
  1   9.463  BB   0.2919 7675.22559  399.94574  46.1388
  2  12.450  BV   0.3205 8959.84277  420.56778  53.8612
```

4.1.1.2 Table S1 – Entry 3 (MeCN, 10 mol% 4, 48 h)

Chiralpak® AD-H, 0.46 × 25 cm, 1 mL/min

80:20 Hex:IPA, 210 nm


```
Signal 1: DAD1 A, Sig=210,8 Ref=off

Peak RetTime Type  Width     Area      Height     Area
 #    [min]        [min]   [mAU*s]     [mAU]       %
----|-------|----|-------|----------|----------|--------|
  1   9.408  BB   0.2869 1.26440e4   686.47675  82.0604
  2  12.409  BV   0.3230 2764.14673  130.57039  17.9396
```

4.1.1.3   Table S1 – Entry 4 (THF, 10 mol% 4, 28 h)

Chiralpak® AD-H, 0.46 × 25 cm, 1 mL/min

80:20 Hex:IPA, 210 nm

DAD1 A, Sig=210,8 Ref=off (NATASHA CH...\NATASHA1_1 2016-01-14 14-06-25\CHIRALPAK ADH 14JAN16 NE3-06-1.D)
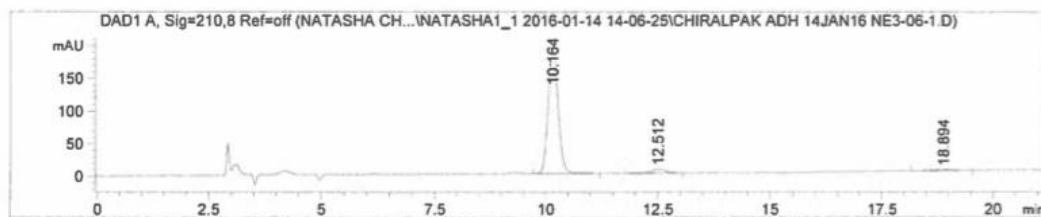
Signal 1: DAD1 A, Sig=210,8 Ref=off

Peak #	RetTime [min]	Type	Width [min]	Area [mAU*s]	Height [mAU]	Area %
1	10.164	BB	0.2367	3027.95068	197.72035	95.1115
2	12.512	BB	0.3103	121.32378	5.98977	3.8109
3	18.894	BB	0.3897	34.30502	1.11280	1.0776

4.2   Optimisation of the reaction conditions for the enantioselective methanolysis of *meso*-cyclic anhydride 2c using organocatalyst 4.

Meso-anhydride **2c** was desymmetrised using the conditions reported previously in tetrahydrofuran (Section S4.4). The presence of catalyst **4** (10 mol%) with anhydrous methanol (10 eq.) in THF afforded the monoesters in good yields (Table S2). The monoester was purified by acid extraction to remove the chiral catalyst, however at times when this was inefficient, column chromatography was performed. The enantioselectivity was increased by using a lower temperature (Table S2, Entry 2) and increasing the loading of the catalyst (Table S2, Entry 3 and Section 5.1.2). The enantioselectivity of the monoesters were deduced by HPLC using a chiral stationary phase.

Table S2: Optimisation of the reaction conditions for the enantioselective methanolysis of *meso*-cyclic anhydride **2c** using organocatalyst **4**.
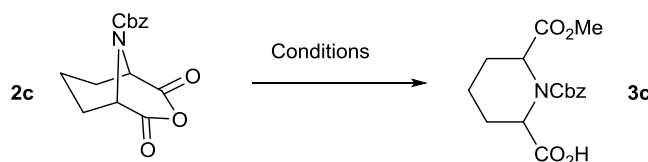
Entry	THF / M	4, MeOH / eq.	T / ^{o}C	t / h	% Yield	% e.e. [a]
1	0.1	0.1, 10	25	48	93	5
2	0.1	0.7, 10	–20	48	91	48
3	0.022	1.1, 1	–20	7	90	96

[a] *e.e.* was determined by HPLC on chiral stationary phase (see Section S4.2.1).

4.2.1 HPLC traces for entries in Table S2

4.2.1.1 Table S1 – Entry 1

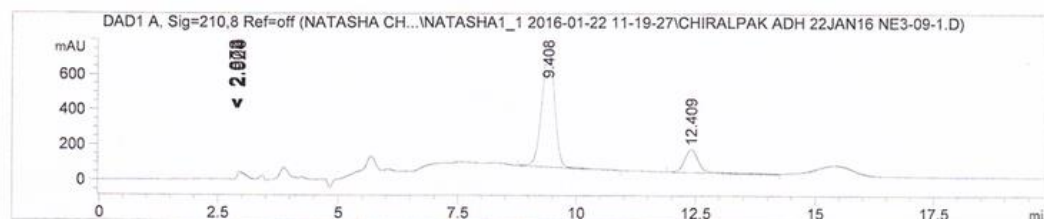Chiralpak® AD-H, 0.46 × 25 cm, 1 mL/min

95:5 Hex:IPA, 210 nm

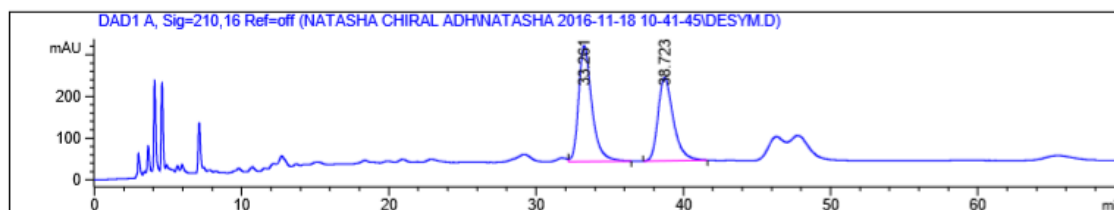DAD1 A, Sig=210,16 Ref=off (NATASHA CHIRAL ADH\NATASHA 2016-11-18 10-41-45\DESYM.D)

Signal 1: DAD1 A, Sig=210,16 Ref=off

Peak #	RetTime [min]	Type	Width [min]	Area [mAU*s]	Height [mAU]	Area %
1	33.261	VB	0.9250	1.73599e4	277.82312	54.7307
2	38.723	BB	1.0451	1.43588e4	199.64822	45.2693

Totals :   3.17187e4   477.47134

4.2.1.2 Table S1 – Entry 2

Chiralpak® AD-H, 0.46 × 25 cm, 0.5 mL/min

95:5 Hex:IPA, 210 nm

DAD1 A, Sig=210,16 Ref=off (NATASHA CHIRAL ADH\NATASHA 2016-09-12 09-10-07\CBZPIPOHOME PURIF.D)
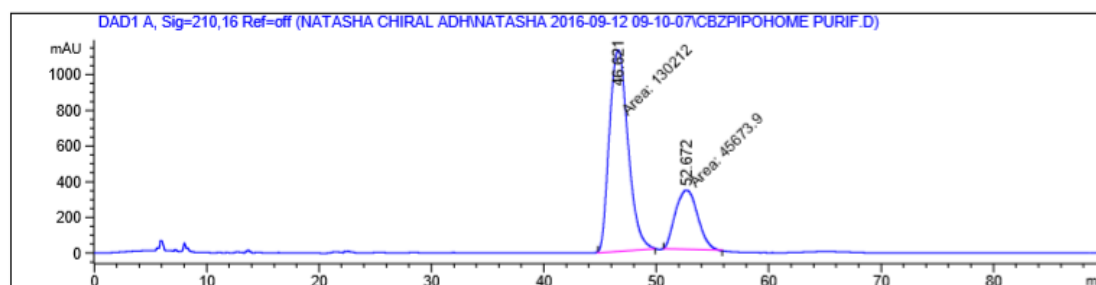
Signal 1: DAD1 A, Sig=210,16 Ref=off

Peak #	RetTime [min]	Type	Width [min]	Area [mAU*s]	Height [mAU]	Area %
1	46.621	MM	1.9208	1.30212e5	1129.85779	74.0321
2	52.672	MM	2.2964	4.56739e4	331.48849	25.9679

Totals :   1.75886e5   1461.34628

5. Determination of the enantiomeric excess (*e.e.*) of 3a, 3b, 3c, 3d and 3e

5.1 Determination of the *e.e.* by HPLC for compounds 3a, 3b and 3d

5.1.1 HPLC trace for (*R*)-naphthylethylamine derivative of scalemic 3a
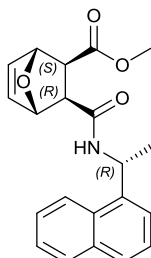
Chiralpak® AD-H, 0.46 × 25 cm, 1 mL/min
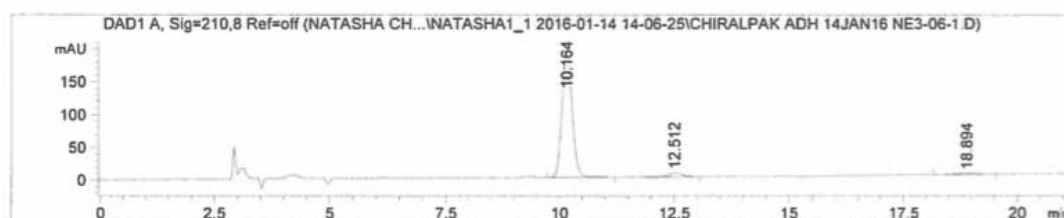
80:20 Hex:IPA, 210 nm


```
Signal 1: DAD1 A, Sig=210,8 Ref=off

Peak RetTime Type  Width     Area       Height    Area
  #   [min]        [min]   [mAU*s]     [mAU]       %
----|-------|----|-------|----------|----------|--------|
  1  10.164 BB   0.2367 3027.95068  197.72035  95.1115
  2  12.512 BB   0.3103  121.32378    5.98977   3.8109
  3  18.894 BB   0.3897   34.30502    1.11280   1.0776
```

5.1.2 HPLC trace for (*R*)-naphthylethylamine derivative of *rac*-3a
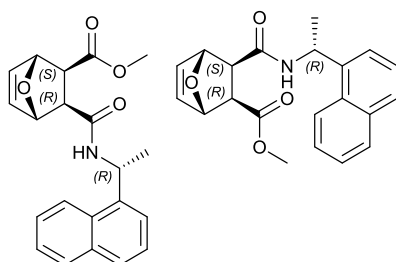
5.1.3 HPLC trace for scalemic 3c

Chiralpak® AD-H, 0.46 × 25 cm, 1 mL/min
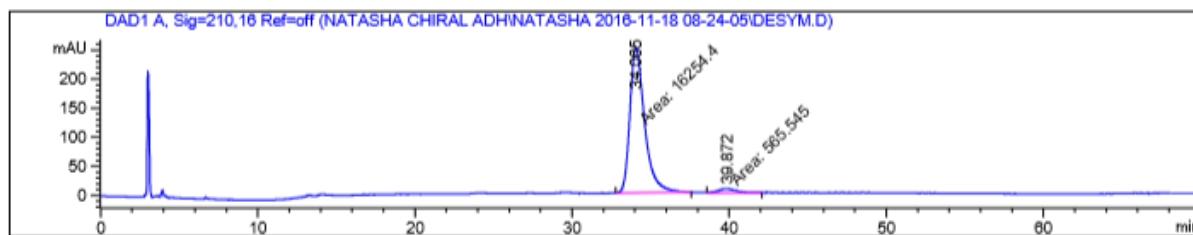
95:5 Hex:IPA, 210 nm


```
Signal 1: DAD1 A, Sig=210,16 Ref=off

Peak RetTime Type  Width     Area      Height    Area
  #   [min]        [min]   [mAU*s]     [mAU]      %
----|-------|----|-------|----------|----------|--------|
  1  34.065 MM   1.0793 1.62544e4   251.00319  96.6377
  2  39.872 MM   1.3538  565.54456    6.96264   3.3623
```
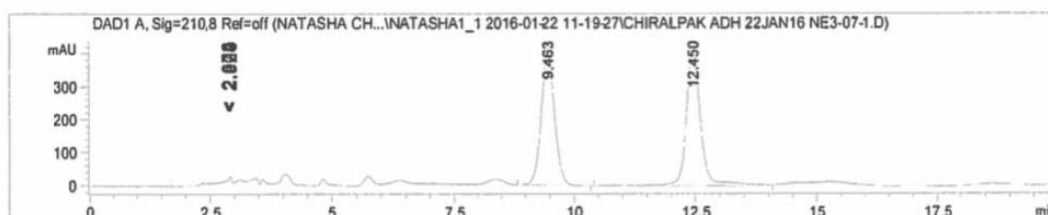
5.1.4 HPLC trace for *rac*-3c
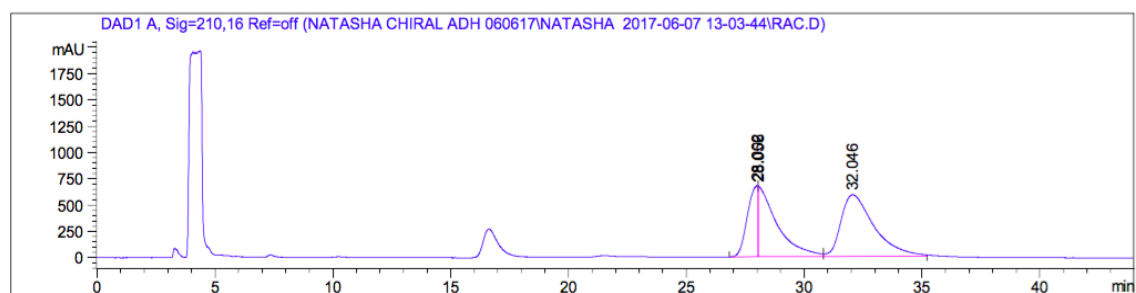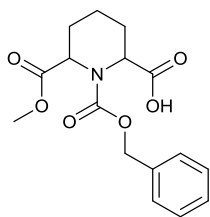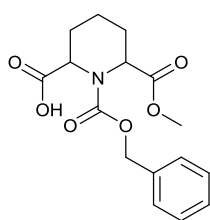
5.1.5 HPLC trace for (*R*)-naphthylethylamine derivative of scalemic 3d

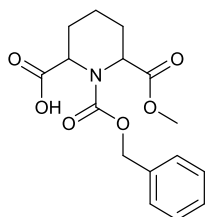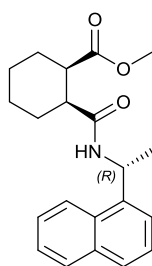Chiralpak® AD-H, 0.46 × 25 cm, 1.2 mL/min

96:4 Hex:EtOH 0.1% TFA, 210 nm
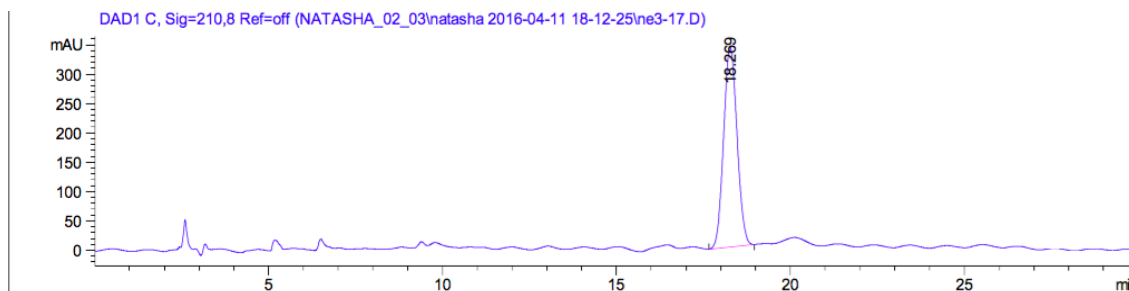

```
Signal 3: DAD1 C, Sig=210,8 Ref=off

Peak RetTime Type  Width     Area      Height     Area
  #   [min]        [min]   [mAU*s]     [mAU]       %
----|-------|----|-------|----------|----------|--------|
  1  18.269 BB    0.4177 9119.50684 341.35202 100.0000
```

5.1.6 HPLC trace for (*R*)-naphthylethylamine derivative of *rac*-3d
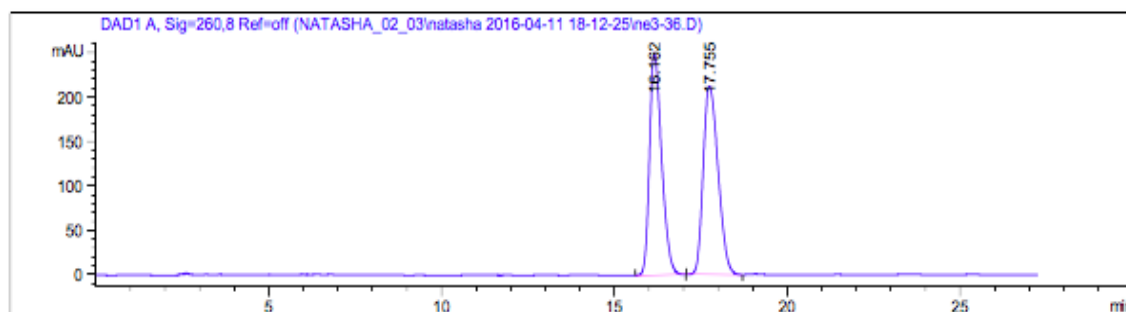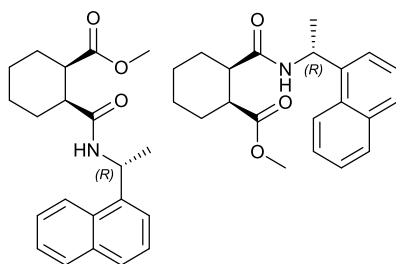
5.2   Determination of the *e.e.* by ^{1}H NMR spectroscopy for compounds 3b and 3e

5.2.1   ^{1}H NMR spectrum for (*R*)-naphthylethylamine derivative of scalemic 3b
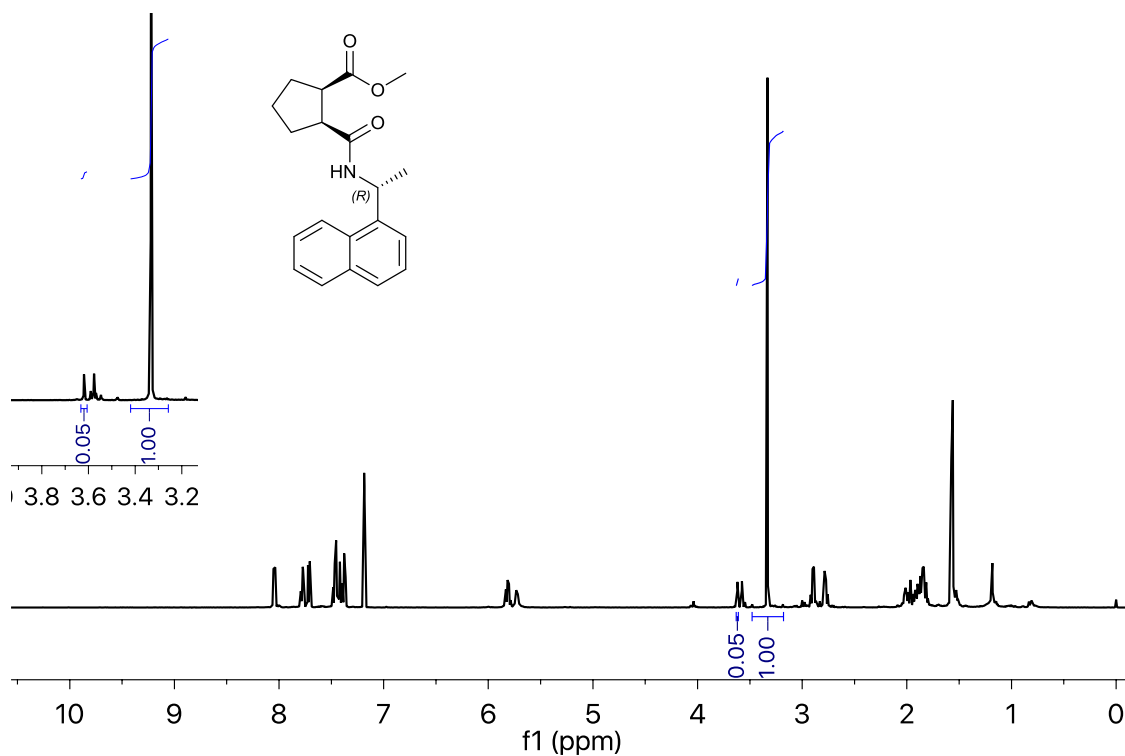
Figure S1: ^{1}H NMR spectrum of the (*R*)-naphthylethylamine derivative of **3b**, which had been formed by methanolysis catalysed by **4**. Inset: Portion of ^{1}H NMR spectrum showing the methyl ester peaks at 3.6 and 3.3 ppm, which indicate a 1.00:0.05 *d.r.*

5.2.2   ^{1}H NMR spectrum for (*R*)-naphthylethylamine derivative of *rac*-3b
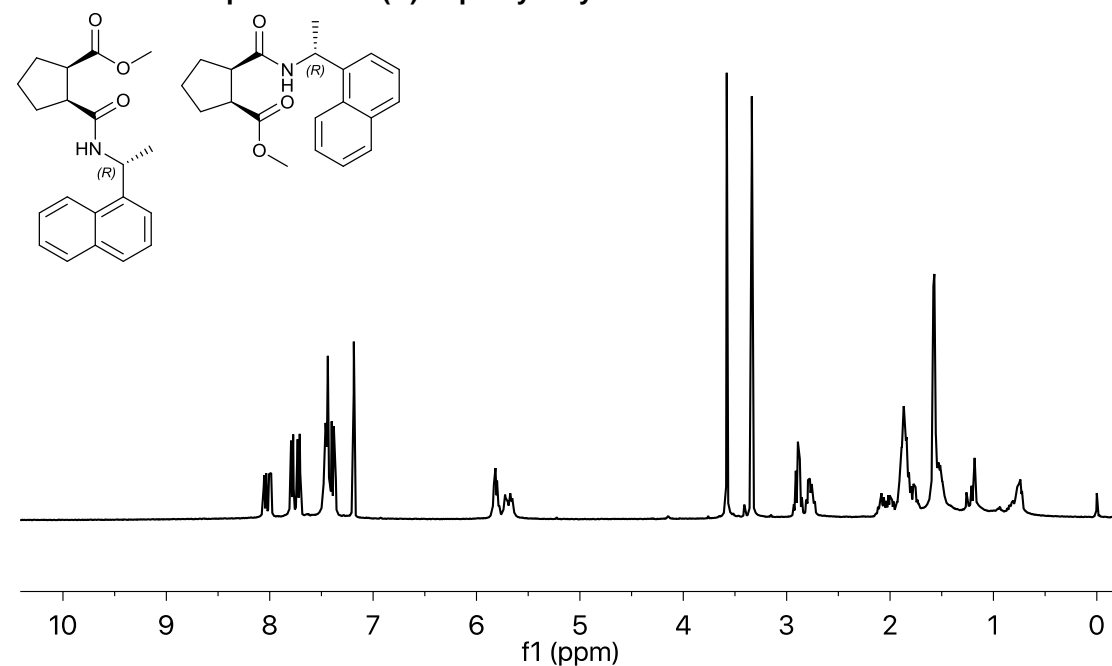
Figure S2: ^{1}H NMR spectrum of the (*R*)-naphthylethylamine derivative of **3b**, which had been formed by uncatalysed methanolysis. Integration of ^{1}H NMR spectrum shows the methyl ester peaks at 3.6 and 3.3 ppm have equal intensity, indicating a 1.00:1.00 *d.r.*

5.2.3 ^{1}H NMR spectrum for (*R*)-naphthylethylamine derivative of scalemic 3e
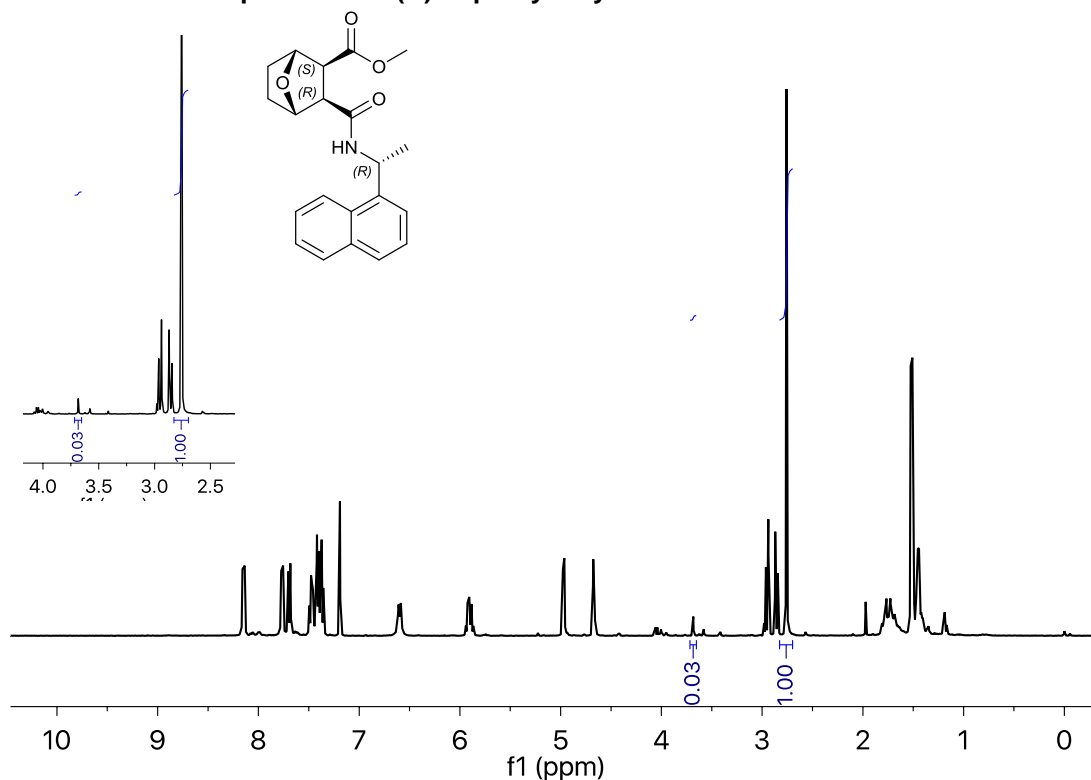
Figure S3: ^{1}H NMR spectrum of the (*R*)-naphthylethylamine derivative of **3e**, which had been formed by methanolysis catalysed by **4**. Inset left: Portion of ^{1}H NMR spectrum showing the methyl ester peaks at 3.7 and 2.75 ppm, which indicate a 1.00:0.03 *d.r.*

5.2.4 ^{1}H NMR spectrum for (*R*)-naphthylethylamine derivative of *rac*-3e
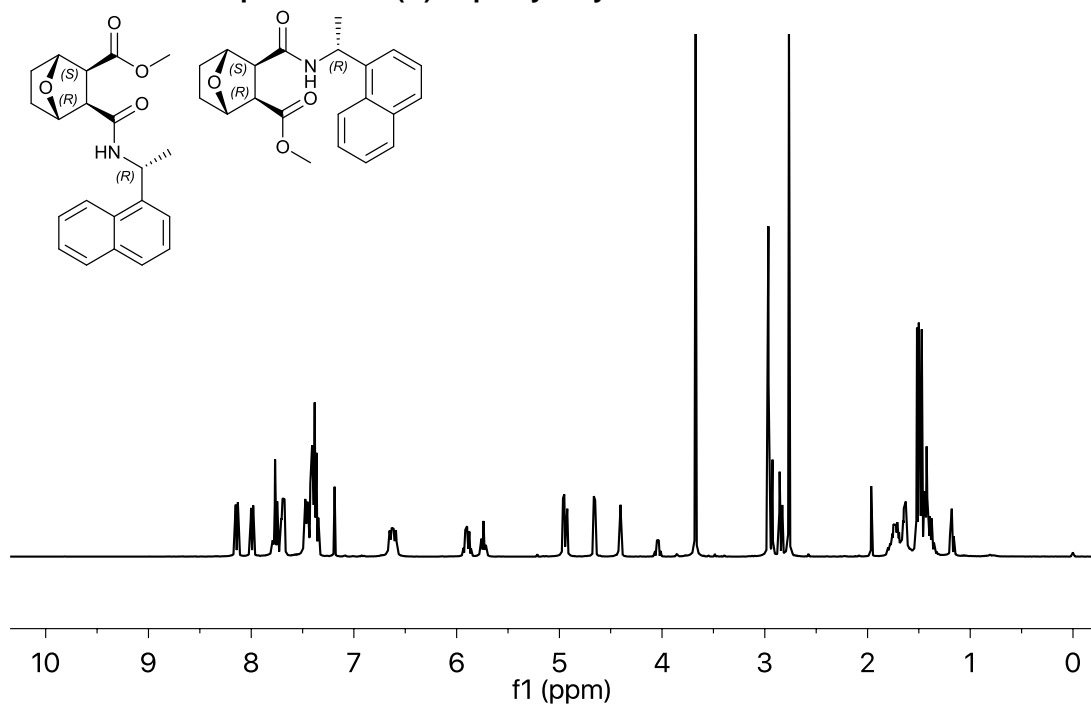
Figure S4: ^{1}H NMR spectrum of the (*R*)-naphthylethylamine derivative of **3e**, which had been formed by uncatalysed methanolysis. Integration of ^{1}H NMR spectrum shows the methyl ester peaks at 3.7 and 2.75 ppm have equal intensity, indicating a 1.00:1.00 *d.r*

6. ^{1}H and ^{13}C NMR spectra of synthesised compounds

6.1.1 Zn(1).2ClO$_4$
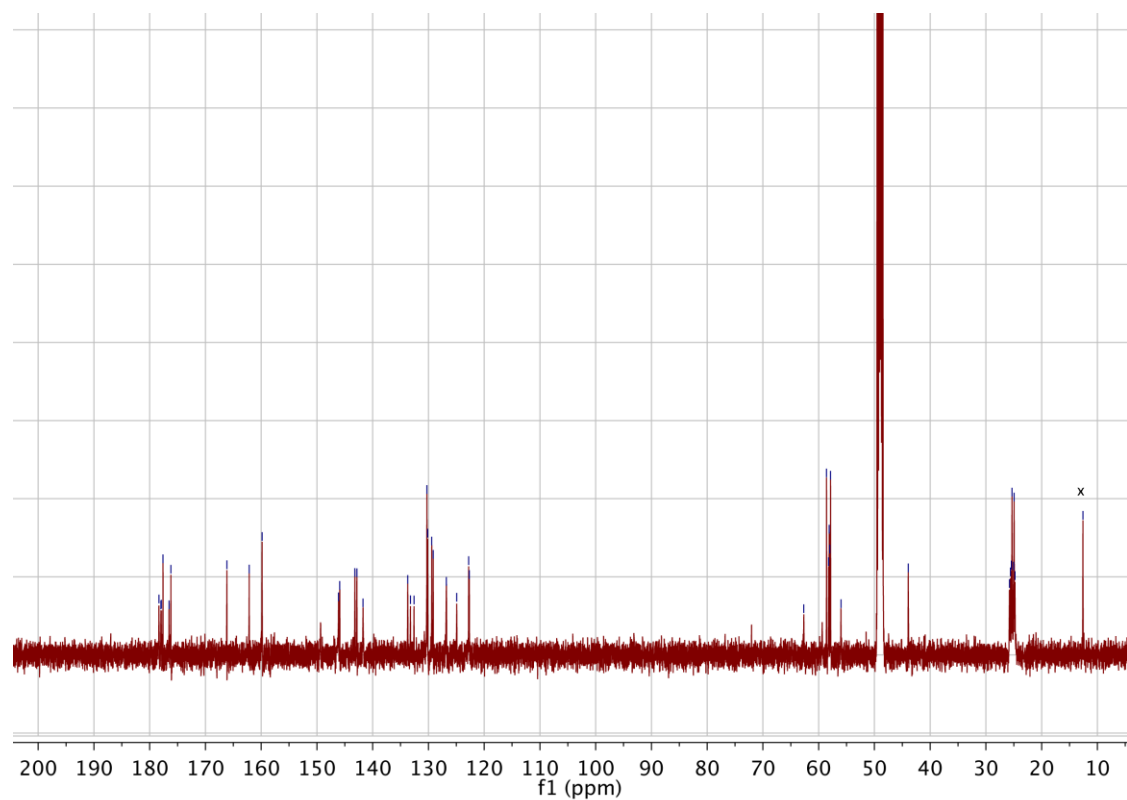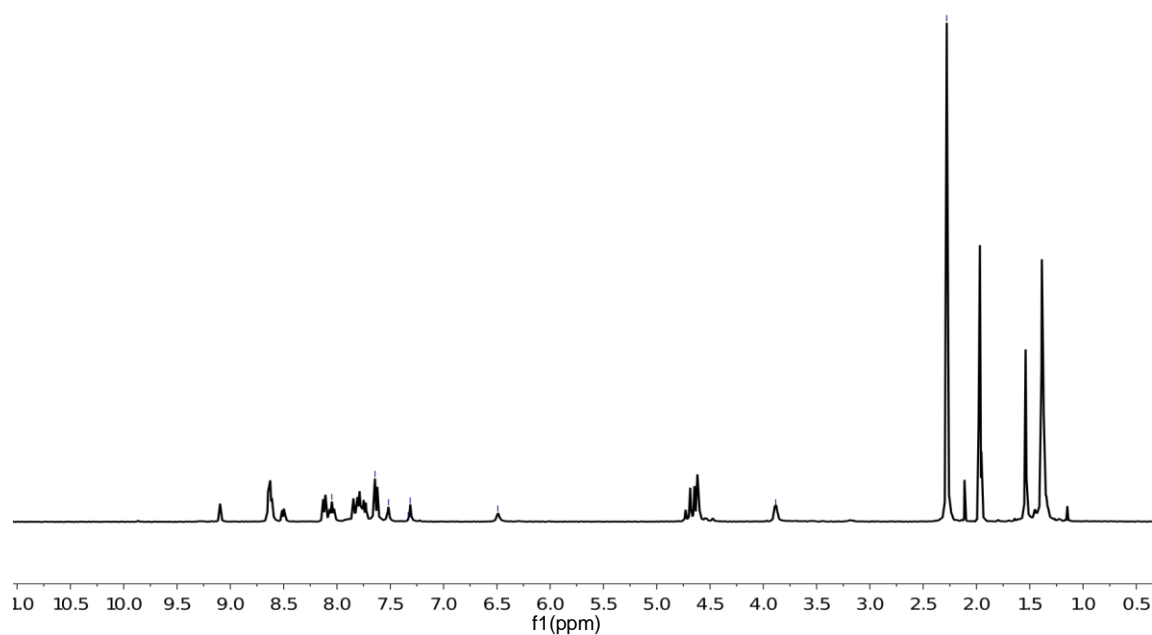
6.1.2 (1*S*,2*R*,3*S*,4*R*)-3-(Methoxycarbonyl)-7-oxabicyclo[2.2.1]hept-5-ene-2-carboxylic acid (3a)
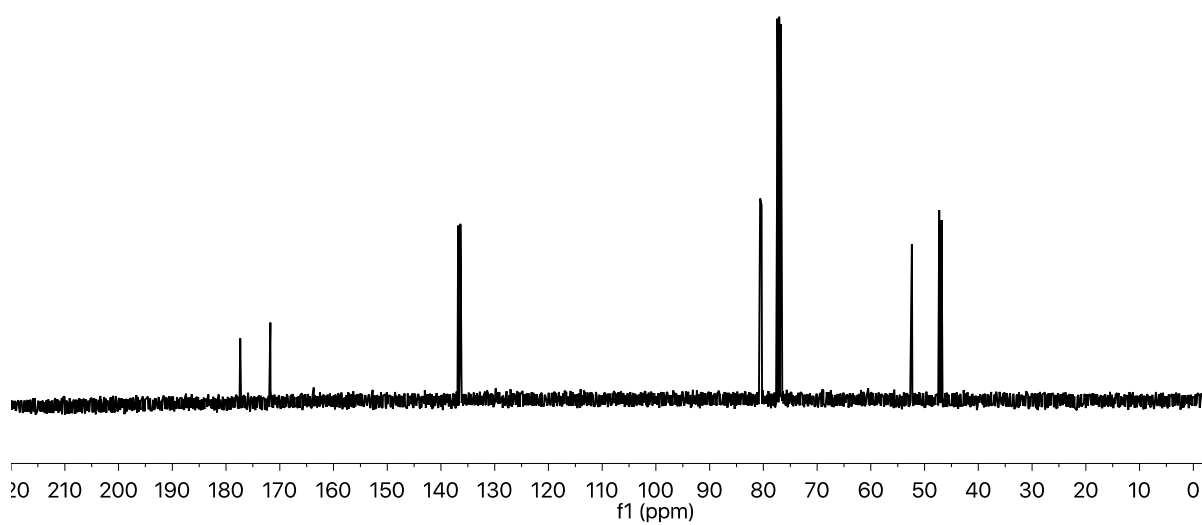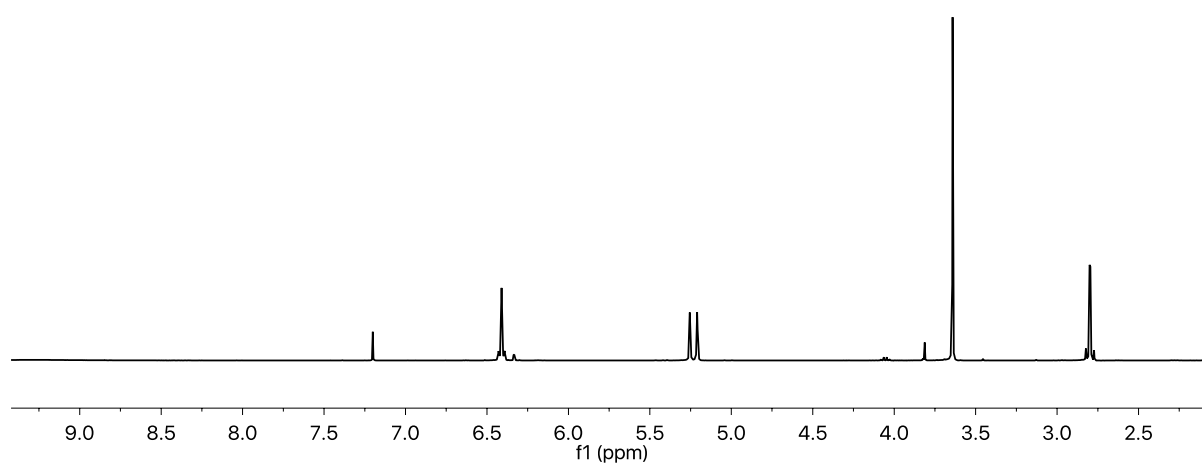
6.1.3   (1*S*,2*R*)-2-(Methoxycarbonyl)cyclopentane-1-carboxylic acid (3b)
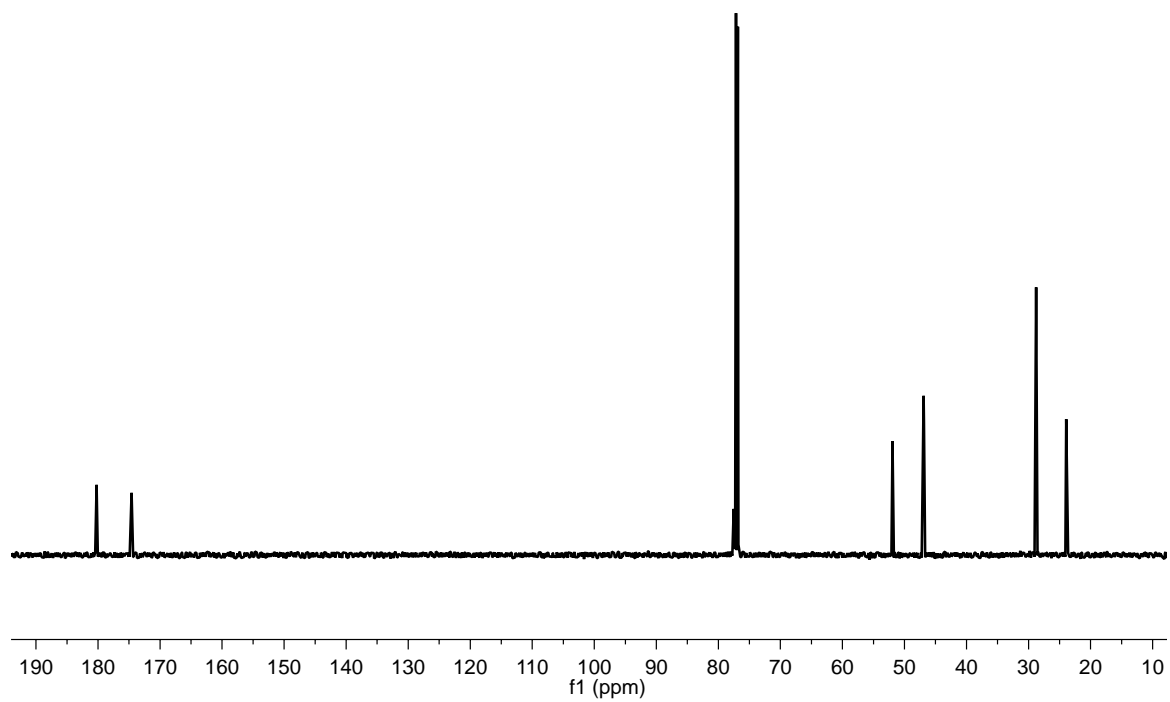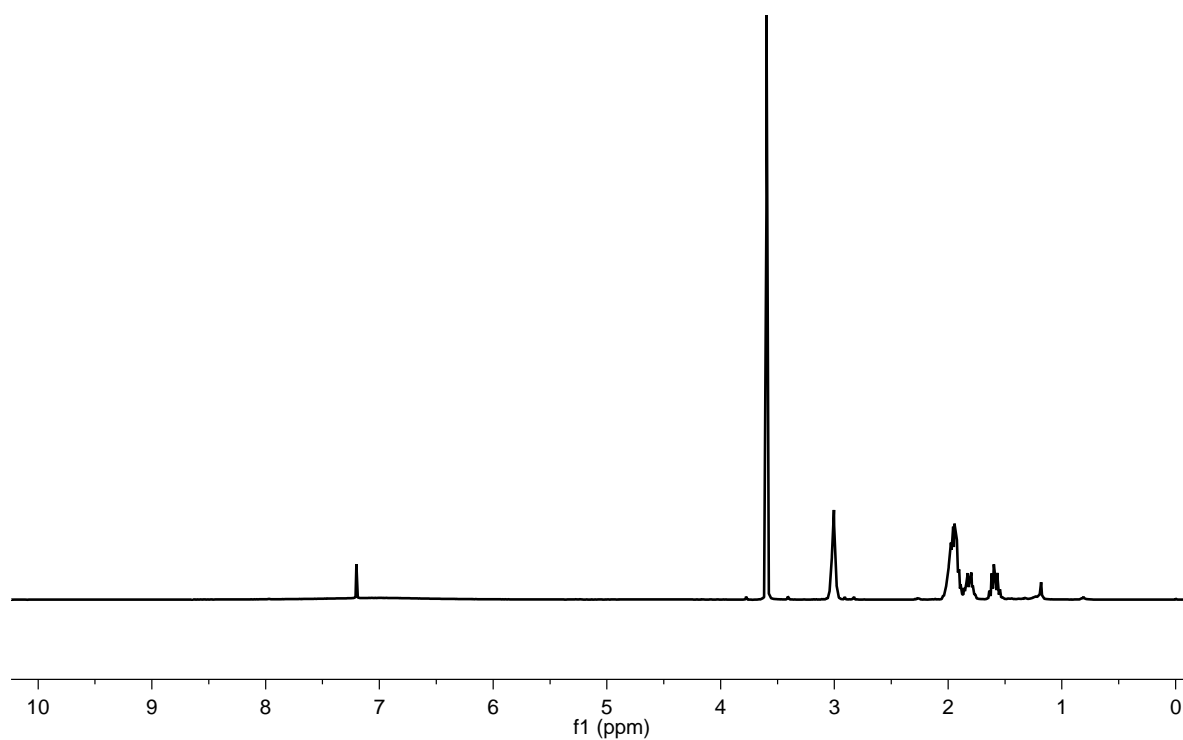
6.1.4 *syn*-1-((Benzyloxy)carbonyl)-6-(methoxycarbonyl)piperidine-2-carboxylic acid (3c)
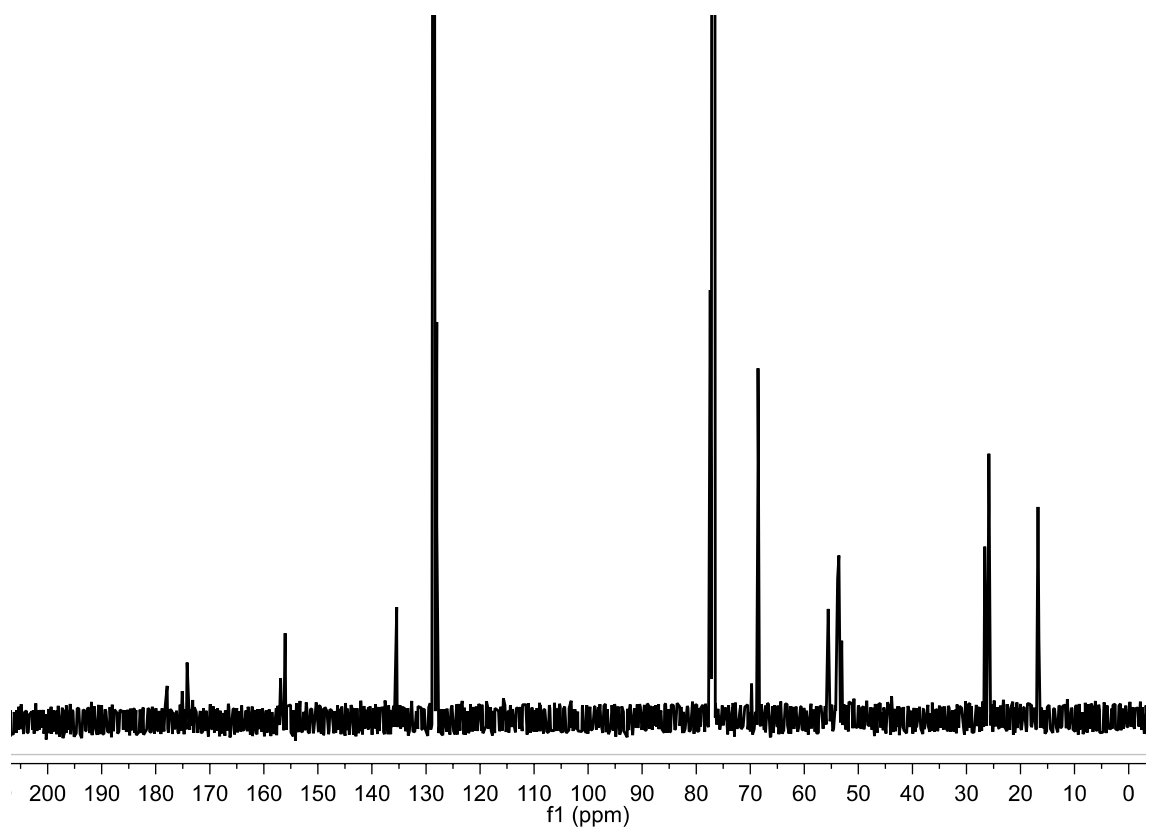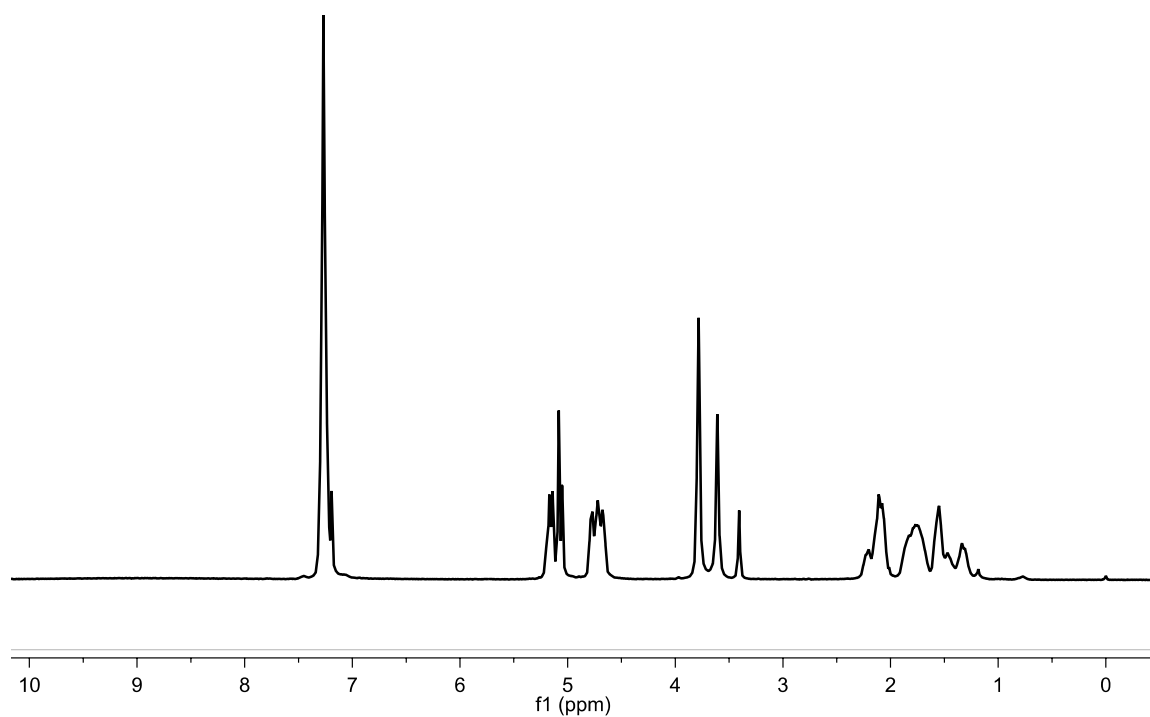
6.1.5 (1*S*,2*R*)-2-(Methoxycarbonyl)cyclohexane-1-carboxylic acid (3d)
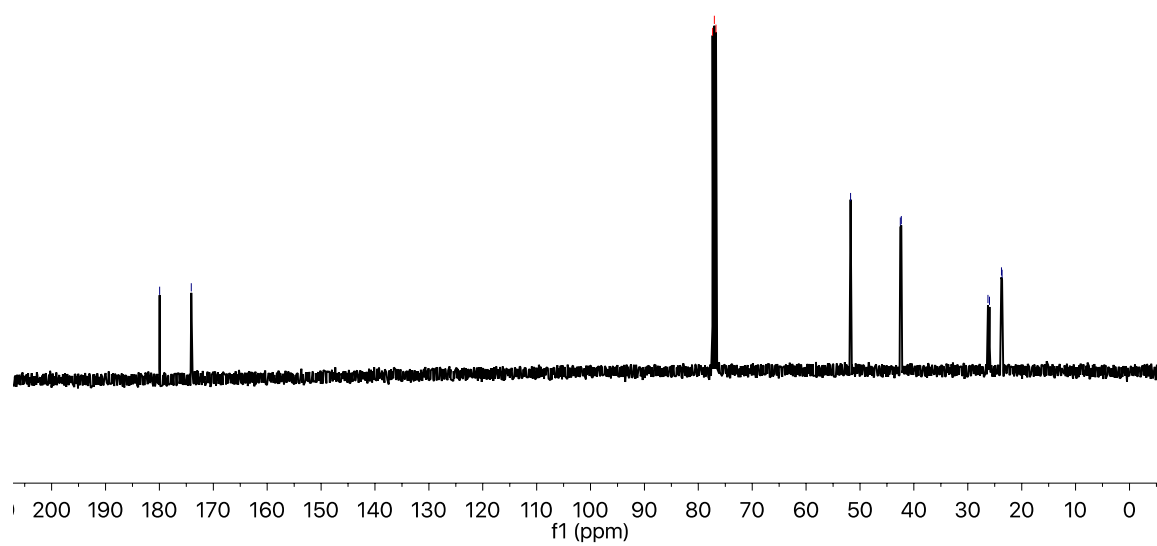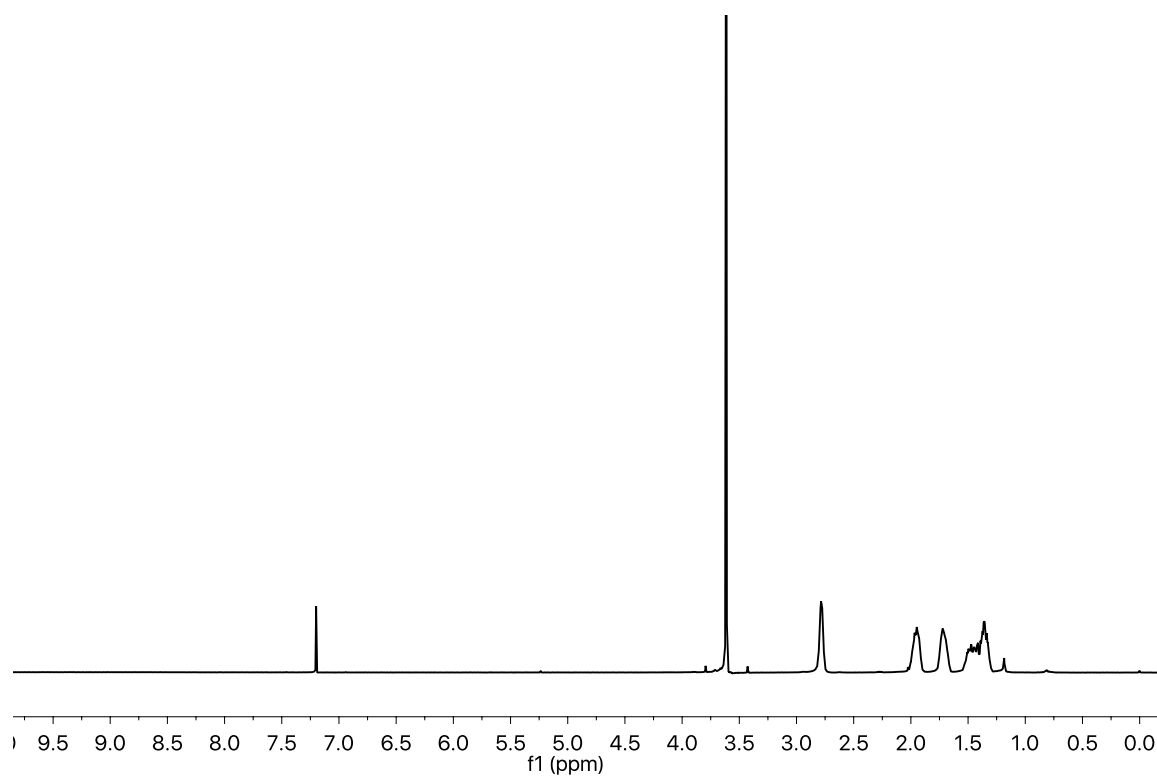
6.1.6 (1*S*,2*R*,3*S*,4*R*)-3-(Methoxycarbonyl)-7-oxabicyclo[2.2.1]heptane-2-carboxylic acid (3e)
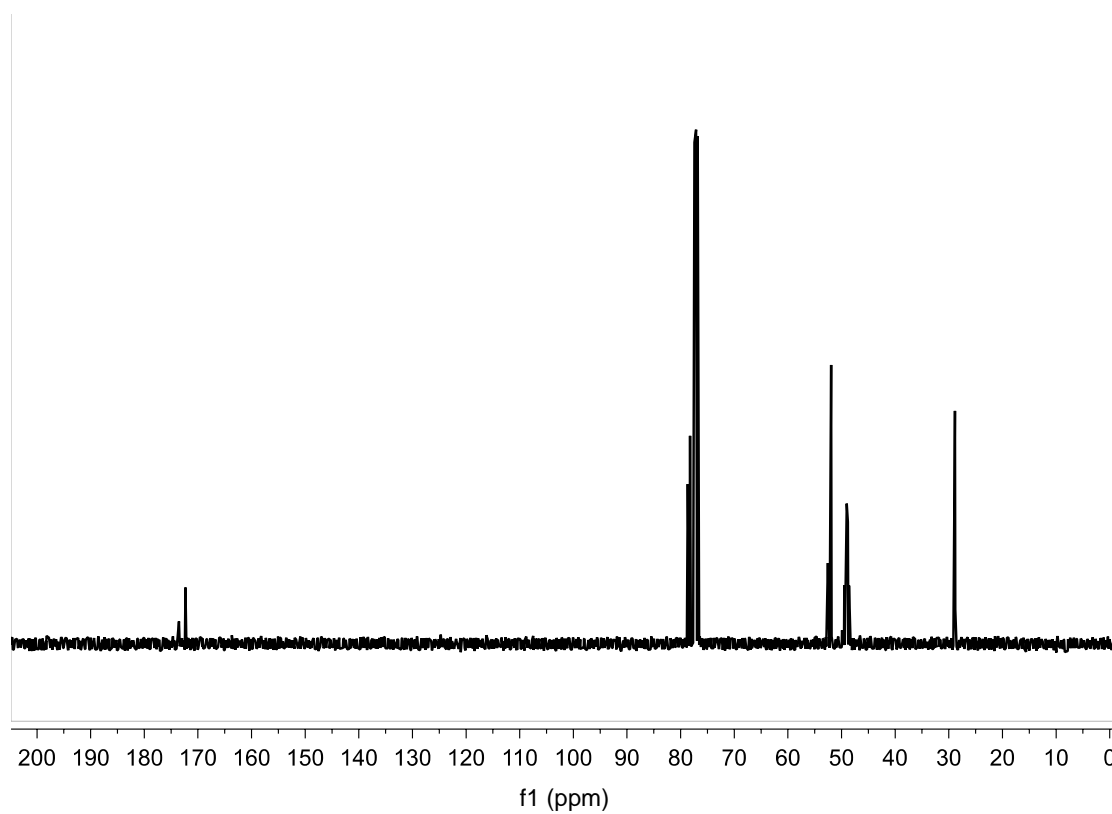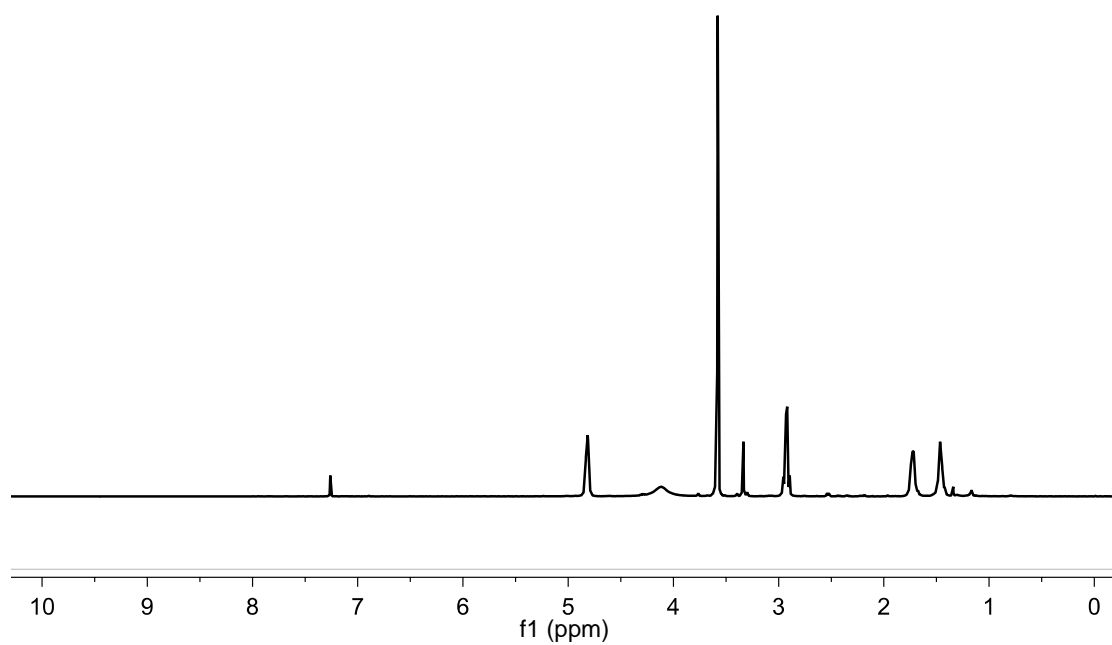
6.1.7 *meso*-Piperidine-2,6-dicarboxylic acid (S2)
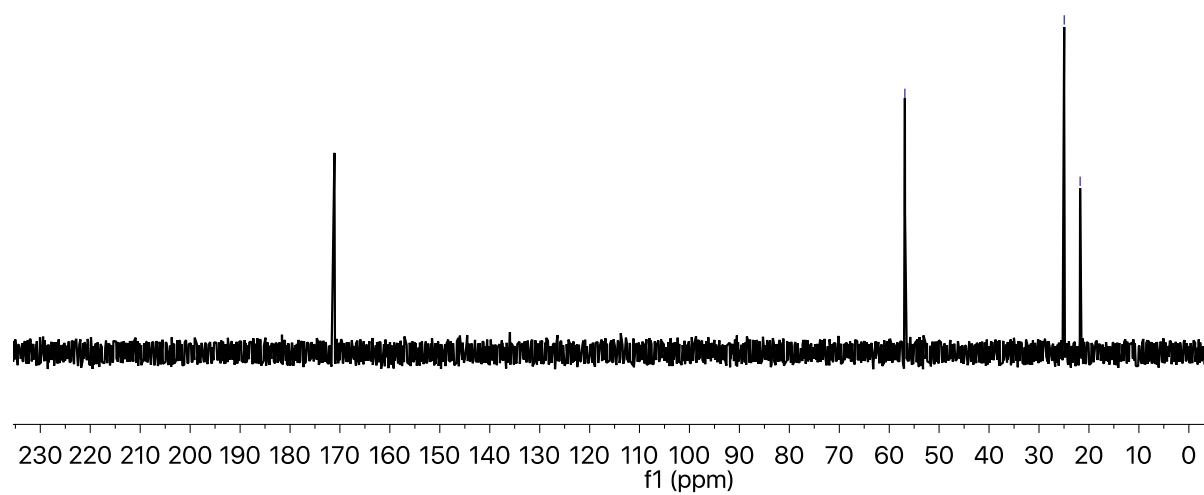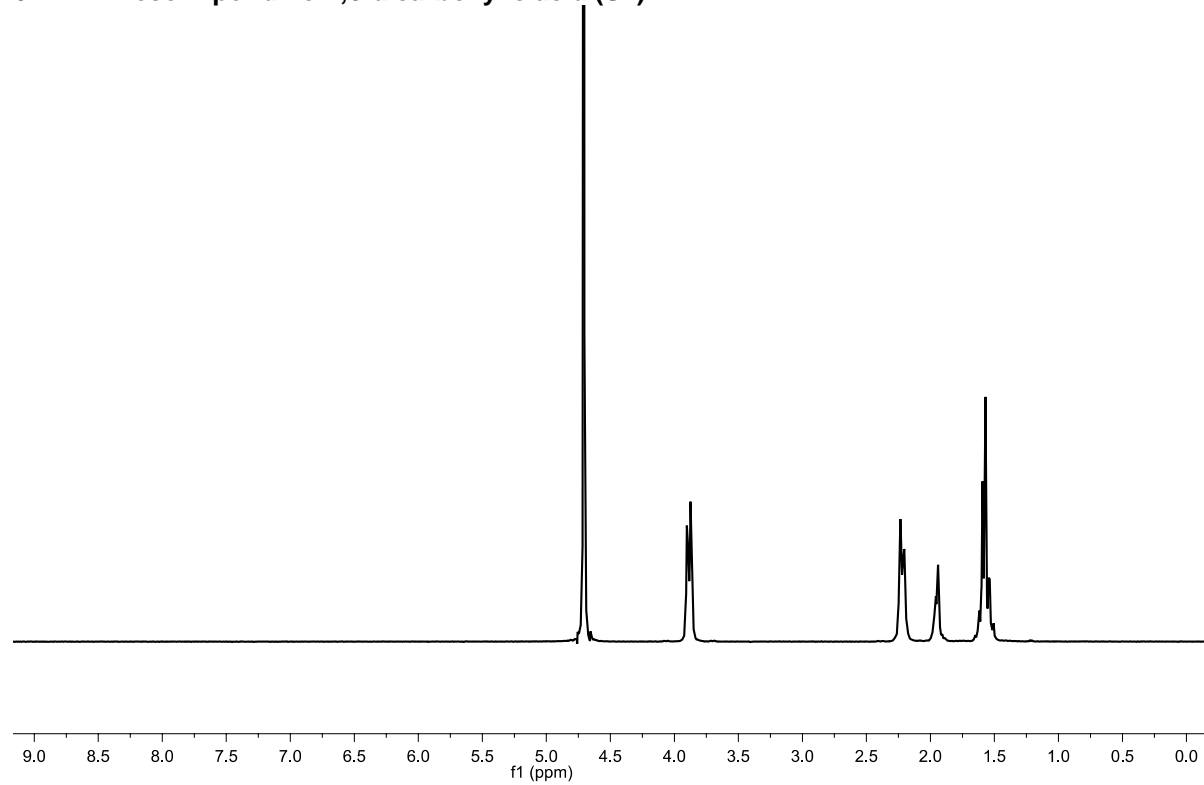
6.1.8   *meso*-1-((Benzyloxy)carbonyl)piperidine-2,6-dicarboxylic acid (S3)
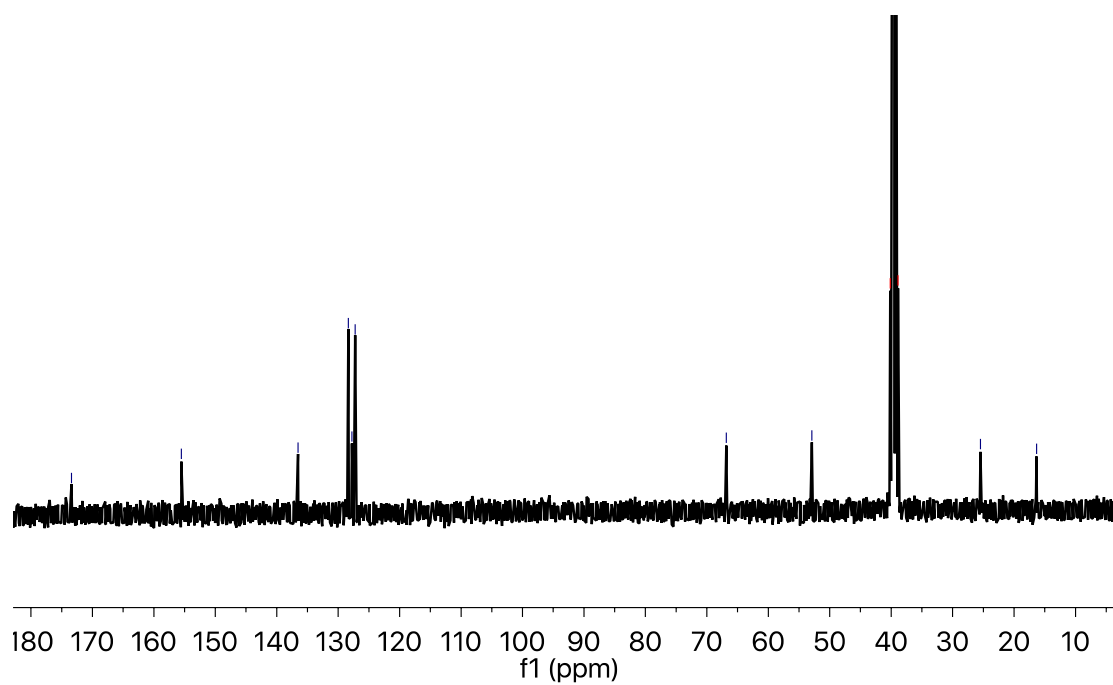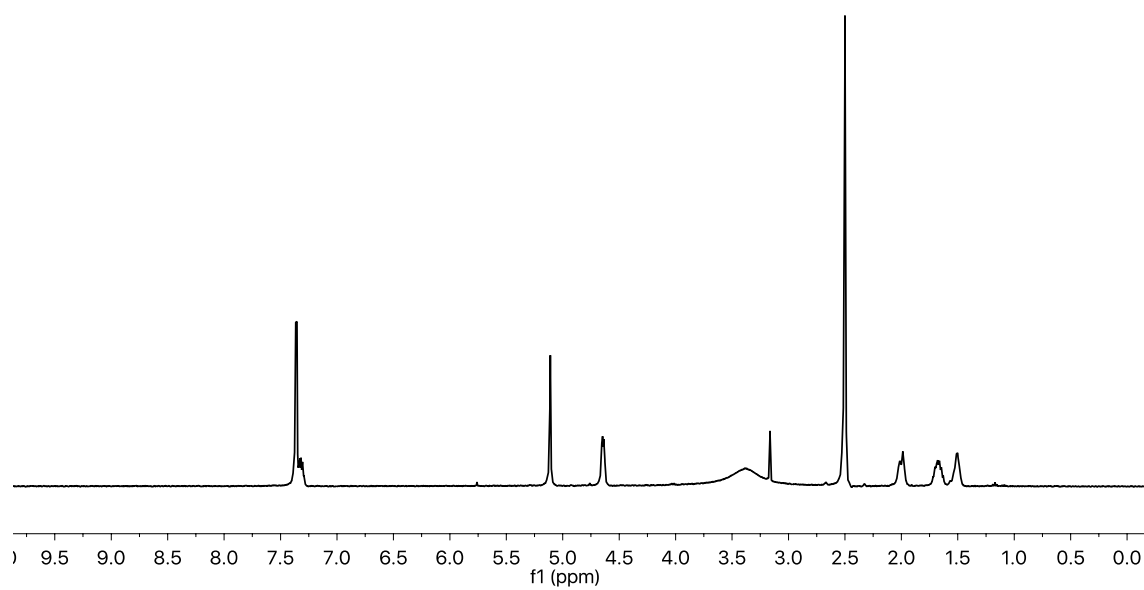
7. NMR spectroscopy studies of Zn(1).2ClO$_4$ in CD$_3$CN

7.1 NMR spectroscopy experimental details

Anhydrous CD$_3$CN and CD$_3$OD, Boc-L-Pro and Boc-D-Pro were obtained from Sigma-Aldrich. Aliquots of stock solutions were added using a Hamilton syringe. The anisochronicity, in parts per billion (ppb), of ABX systems arising from the geminal ^{1}H nuclei of the GlyNH$_2$ diastereotopic NMR probe was given by $u_0\Delta\delta$ (ppb) = $[(((f_{A1}+f_{A2})/2)-((f_{B3}+f_{B4})/2))^*(((f_{A3}+f_{A4})/2)-((f_{B1}+f_{B2})/2))]^{1/2} \times 1000$ where $f_{A1,A2,A3,A4,B1,B2,B3,B4}$ are the observed resonant frequencies in order of the eight lines comprising of the ABX multiplet. Variable temperature NMR (VT-NMR) spectra of Zn(**1**).2ClO$_4$ bound with Boc-L-Pro or *rac*-BocPro were acquired from –40 °C to 40 °C in CD$_3$CN and –50 °C to 40 °C in CD$_3$OD.

7.2 Complexation study: titration of Zn(1).2ClO$_4$ with Boc-L-Pro, 2,6 lutidine in CD$_3$CN

A stock solution of Boc-L-Pro was made by dissolving the carboxylate (75 µmol) and 2,6-lutidine (90 µmol) in CD$_3$CN (1 mL). A stock solution of the host (15 mM) was made by dissolving Zn(**1**).2ClO$_4$ (75 µmol) in CD$_3$CN (5 mL). An aliquot of the host stock solution was added to a NMR tube (500 µL, 7.5 µmol) and a NMR spectrum was acquired for reference. For monitoring the binding of carboxylate to Zn(**1**).2ClO$_4$, aliquots of Boc-L-Pro solution (25 µL = 0.25 eq. acid, 0.3 eq. 2,6-lutidine) were sequentially added and a spectrum was acquired after each addition until 30 µmol of carboxylate and 36 µmol of 2,6-lutidine were added.

The ^{1}H NMR spectrum after the addition of 0.25 and 0.5 equivalents of Boc-L-Pro to Zn(**1**).2ClO$_4$ (Figure S5b) shows well-resolved and sharp resonances corresponding to Zn(**1**).2ClO$_4$ both with and without bound carboxylate, consistent with slow exchange between free and complexed foldamer.

The binding of the chiral 'controller' Boc-L-Pro can be observed in the quinoline aromatic and methylene protons. On binding, the equivalent aromatic quinoline protons become non-equivalent and anisochronicity is observed with both quinolines now being identified individually. This was most noticeable for proton *A* of the quinoline rings that spits into two separate systems (*a* and *a'*) displaying as doublets. The quinoline methylene protons (*G*) that exist as an averaged AB-type system before binding also split further into two separate systems (*g* and *g'*), exhibiting as two ABX-type systems (highlighted blue, Figure S5b).

The transmission of the chiral influence through the helix can be detected at the methyl groups at each Aib residue. The singlet peaks arising from the methyl groups on each Aib split into two separate singlets (for each CH$_3$) due to the chiral controller rendering the methyl groups diastereotopic.

Finally, the output can be detected at the glycinamide residue by the appearance of anisochronicity. The glycinamide protons (highlighted red, Figure S5b) appear as an ABX-type system due to coupling with the adjacent NH.
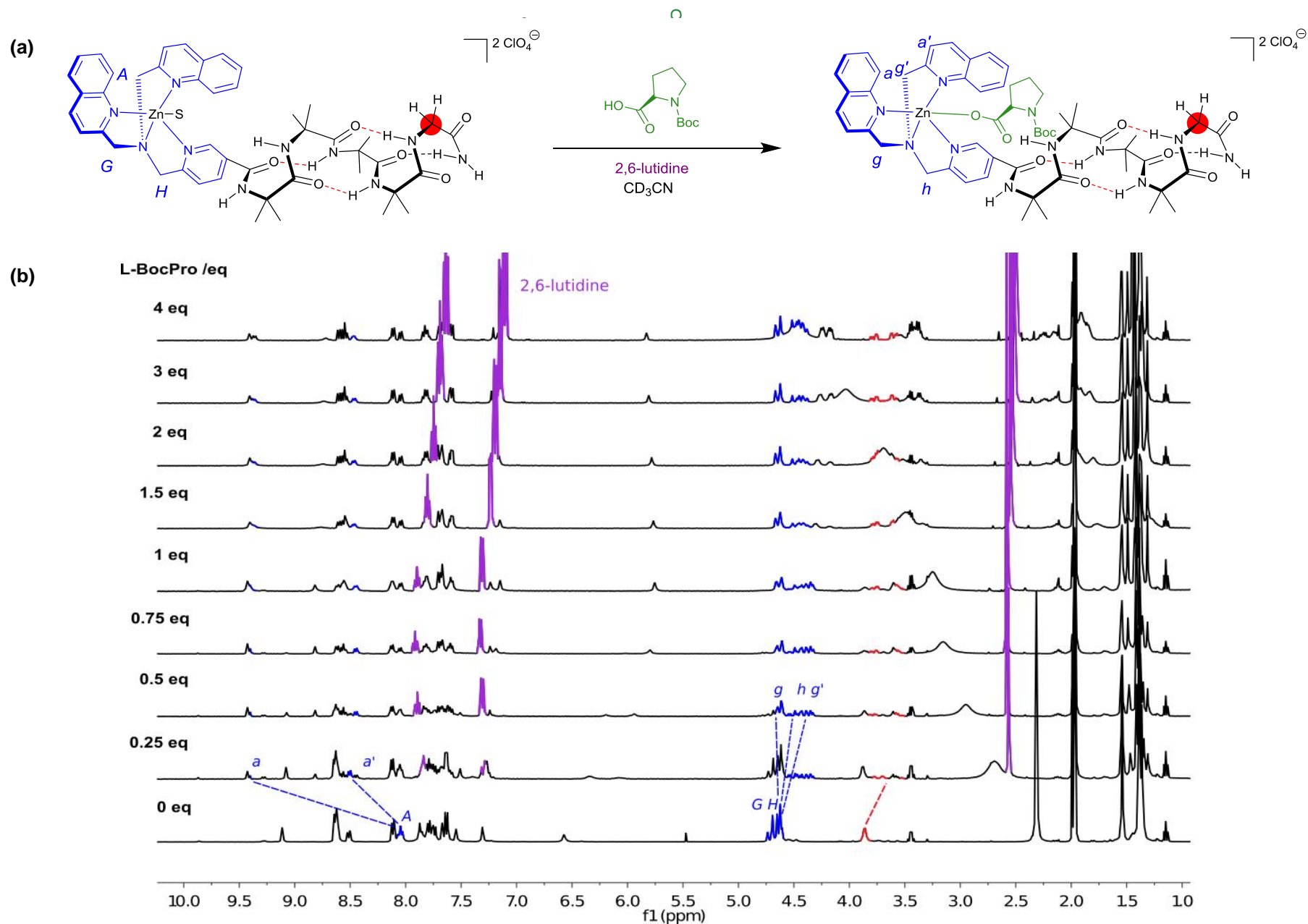
Figure S5: (a) Schematic representation of the binding of Boc-L-Pro with key protons labelled. **(b)** NMR titration of Boc-L-Pro (up to 4 eq.) with Zn(**1**).2ClO₄ in basic CD₃CN (2,6-lutidine, up to 4.8 eq.) in CD₃CN (400 MHz, 298 K). GlyNH₂ reporter highlighted red and 2,6-lutidine is highlighted in purple.

7.3 Complexation study: titration of Zn(1).2ClO$_4$ with *rac*-BocPro, 2,6 lutidine in CD$_3$CN

A stock solution of *rac*-BocPro was made up by dissolving Boc-L-Pro (37.5 µmol), Boc-D-Pro (37.5 µmol) and 2,6-lutidine (90 µmol) in CD$_3$CN (1 mL). A stock solution of the host (15 mM) was made by dissolving Zn(1).2ClO$_4$ (75 µmol) in CD$_3$CN (5 mL). An aliquot of the host stock solution was added to a NMR tube (500 µL, 7.5 µmol) and a NMR spectrum was acquired for reference. For monitoring the binding of carboxylate to Zn(1).2ClO$_4$, aliquots of *rac*-BocPro solution (25 µL = 0.25 eq. acid, 0.3 eq. base) were sequentially added and a spectrum was acquired after each addition until 30 µmol of carboxylate and 36 µmol of 2,6-lutidine were added.

As expected, up to the addition of one equivalent of carboxylate, both carboxylate-bound and solvent-bound species were identifiable in the ^{1}H NMR spectra with relatively sharp peaks. Interestingly, the spectra of the mixtures with less than 1 eq. of the racemate present are broader than the corresponding spectra for the addition of <1 eq. Boc-L-Pro, suggesting that any exchange processes (i.e. interchange of coordinated Boc-L-Pro for Boc-D-Pro) may be faster when there is an excess of carboxylate present. Above 1 equivalent, instead of anisochronicity being observed at the glycinamide as with the Boc-L-Pro controlled foldamer, the glycinamide had the appearance similar to that of the solvent bound foldamer (Figure S6 and S7b). A small doublet (owing to the coupling of the methylene protons to the adjacent NH) was observed instead of an ABX-type system. Anisochronicity was also absent at the aromatic quinolines and quinolyl methylene protons. A broad singlet was observed for the quinolyl methylene protons instead of two ABX-systems that are observed for the Boc-L-Pro controlled foldamer.
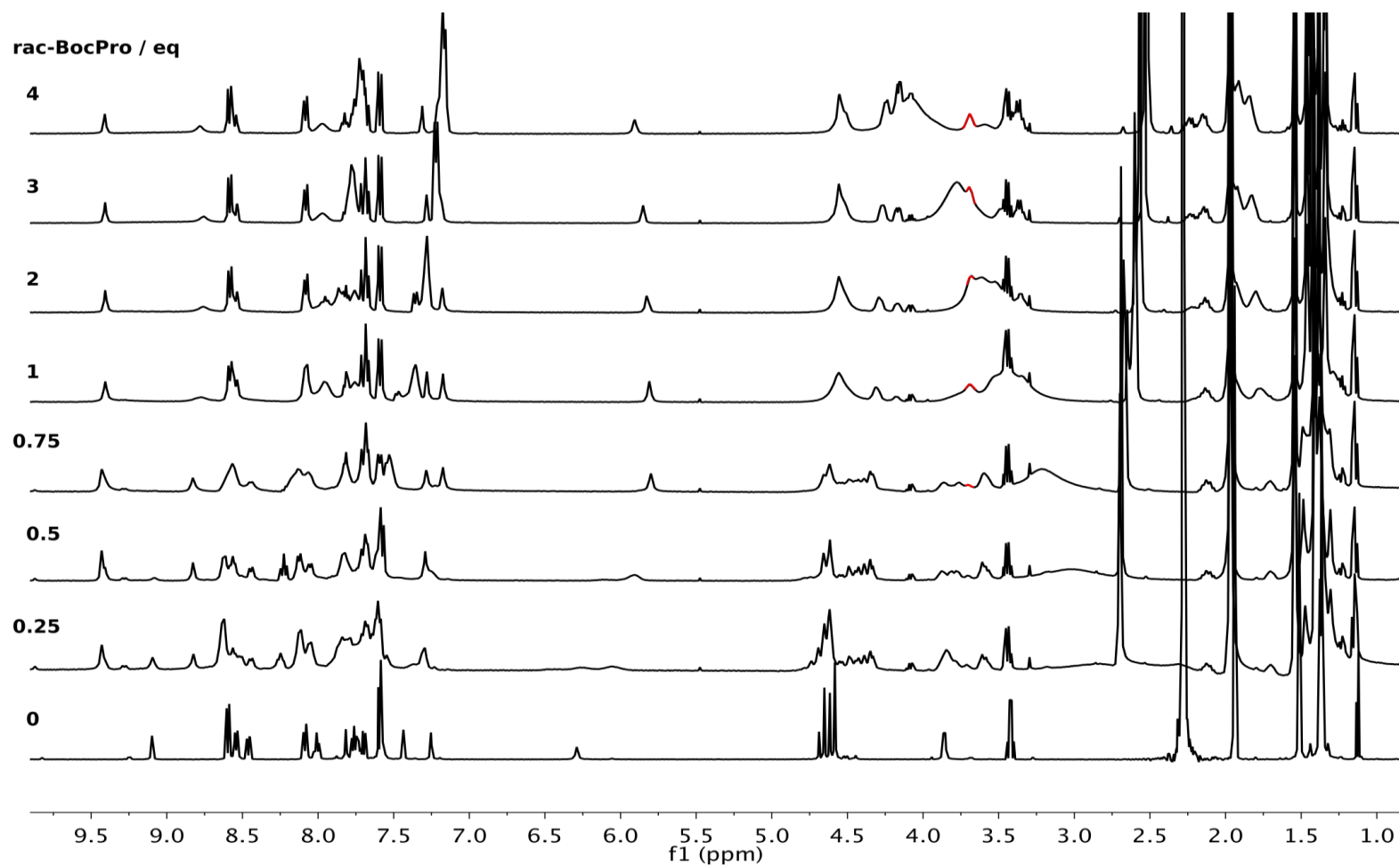
Figure S6: NMR titration of *rac*-BocPro (up to 4 eq.), 2,6-lutidine (up to 4.8 eq.) and Zn(**1**).2ClO$_4$ in CD$_3$CN (400 MHz, 298 K). GlyNH$_2$ reporter highlighted in red.

7.4 Comparison of the spectral changes during titration of Zn(1).2ClO₄ with either Boc-L-Pro or *rac*-BocPro (with 2,6 lutidine) in CD₃CN.
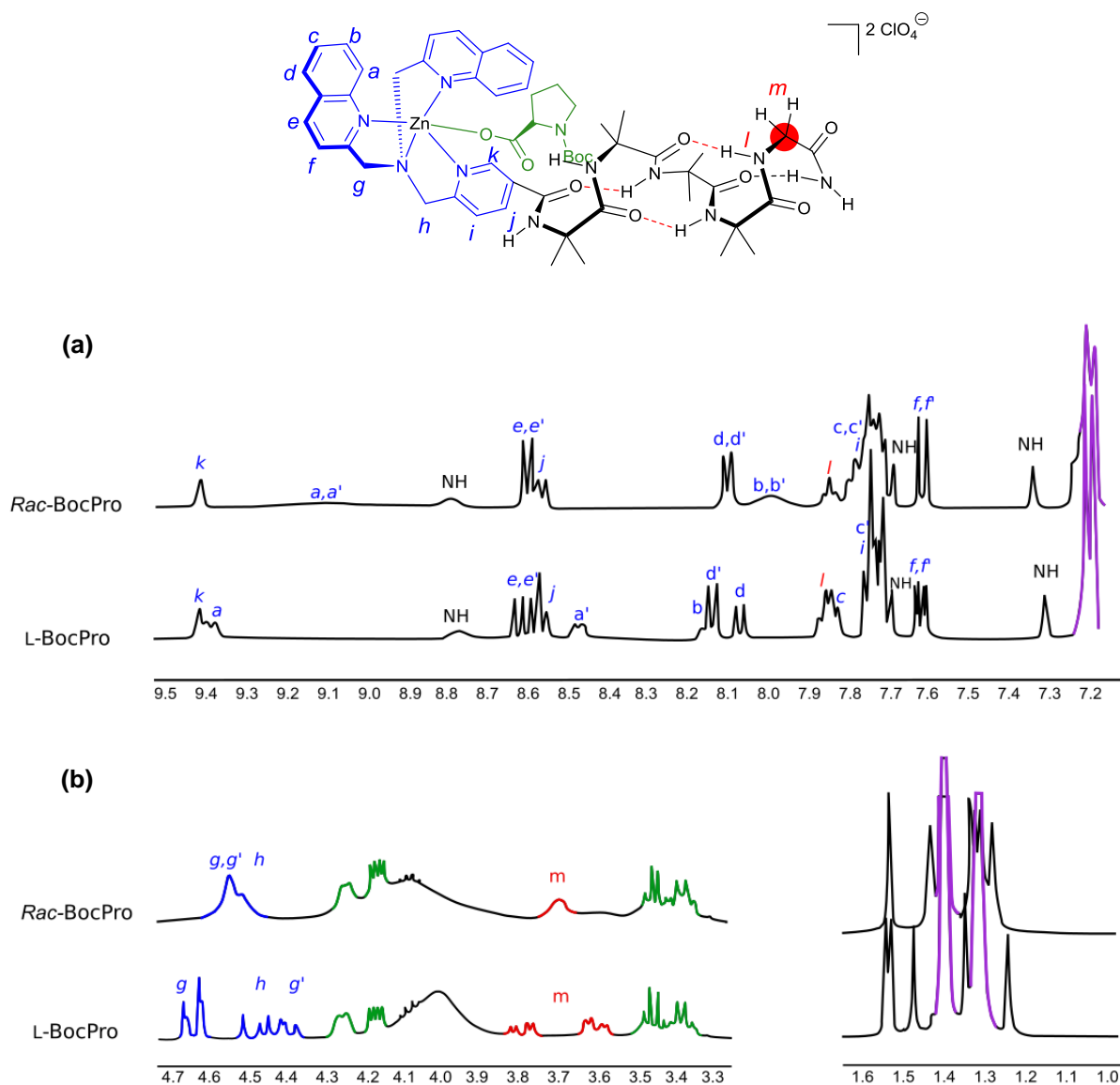
Figure S7: Expansions of the ^{1}H NMR spectra of Zn(**1**).2ClO₄ bound to Boc-L-Pro (2 eq.) or *rac*-BocPro (2 eq.) in CD₃CN. Anisochronicity of the glycinamide probe and the quinolyl methylene protons is highlighted in red and blue respectively. Green resonances correspond to BocPro and the purple resonances correspond to 2,6-lutidine. **(a)** Region from 7.1 to 9.5 ppm. **(b)** Regions 3.3 to 4.7 ppm and 1.0 to 1.6 ppm.

These complexation assays suggest that Zn(**1**).2ClO₄ (*rac*-BocPro controlled) exists as two species, Boc-D-Pro bound and Boc-L-Pro bound, that independently induce their stereocontrol on Zn(**1**).2ClO₄. Their magnitude of control is equivalent, but the Boc-L-Pro bound [Zn^II(BQPA)]-foldamer induces a left-handed helical conformation whilst the Boc-D-Pro bound [Zn^II(BQPA)]-foldamer induces a right-handed helical conformation. The anisochronicity that arises from these two diastereotopic conformations is lost in the weighted average signal, with broad signals being observed in some cases. It is thought that interconversion between

Boc-D-Pro and Boc-L-Pro at the Zn(II) metal centre must be fast on the ^{1}H NMR spectroscopy timescale, leading to weighted average peaks being observed. Two suggested mechanisms for this process are shown in Figure S8, which either involve complexation of free carboxylate to give a hexa-coordinate intermediate or the formation of dimeric Zn(II) complexes that have bridging carboxylates. The appearance of some weak anisochronicity at <1 equivalents of added *rac*-BocPro could suggest the former, with free (uncomplexed) carboxylate mediating the exchange processes.

(a)

Zn(MeOH)(**1**)$^{2+}$ D-BocPro   Zn(D-BocPro)(**1**)$^{+}$
racemic   **slow**   *P helix favoured*

L-BocPro **slow**   Zn(L-BocPro)(**1**)$^{+}$ **fast**

Zn(D-BocPro)(**1**)$^{+}$

Zn(L-BocPro)(**1**)$^{+}$ **fast**   [Zn(**1**)]$_2$(D-BocPro)(L-BocPro)
M helix favoured   *Dimeric intermediate with hexa-coordinate Zn(II) centres and bridging carboxylates*

(b)

Zn(MeOH)(**1**)$^{2+}$ D-BocPro   Zn(D-BocPro)(**1**)$^{+}$
racemic   **slow**   *P helix favoured*

L-BocPro **slow**   L-BocPro **fast**

D-BocPro

Zn(L-BocPro)(**1**)$^{+}$ **fast**   Zn(D-BocPro)(L-BocPro)(**1**)
M helix favoured   *Six-coordinate racemic intermediate*

Figure S8: Two proposed mechanisms for the interchange of Zn(**1**)-bound BocPro that might be fast on the ^{1}H NMR spectroscopy timescale.

7.5 Titration of Zn(1).2ClO$_4$ with scalemic mixtures of BocPro and 2,6 lutidine in CD$_3$CN

A stock solution of the host (15 mM) was made by dissolving Zn(**1**).2ClO$_4$ (75 µmol) in CD$_3$CN (5 mL). Stock solutions of Boc-L-Pro (75 mM) and Boc-D-Pro (75 mM) were made up by dissolving the required carboxylate (75 mmol) and 2,6-lutidine (90 mmol) in CD$_3$CN (1 mL). Scalemic mixtures of BocPro (40%, 50%, 60%, 70%, 80% and 90%) were made by mixing aliquots of Boc-D-Pro stock solution and Boc-L-Pro solution to give scalemic mixtures of BocPro at 75 mM. Each NMR spectrum acquired was a separate solution containing 500 µL of Zn(**1**).2ClO$_4$ (7.5 µmol), and 200 µL of the required BocPro scalemic mixture (15 µmol, 2 eq. of acid, 2.4 eq. of base). Anisochronicity at the glycinamide probe was measured.
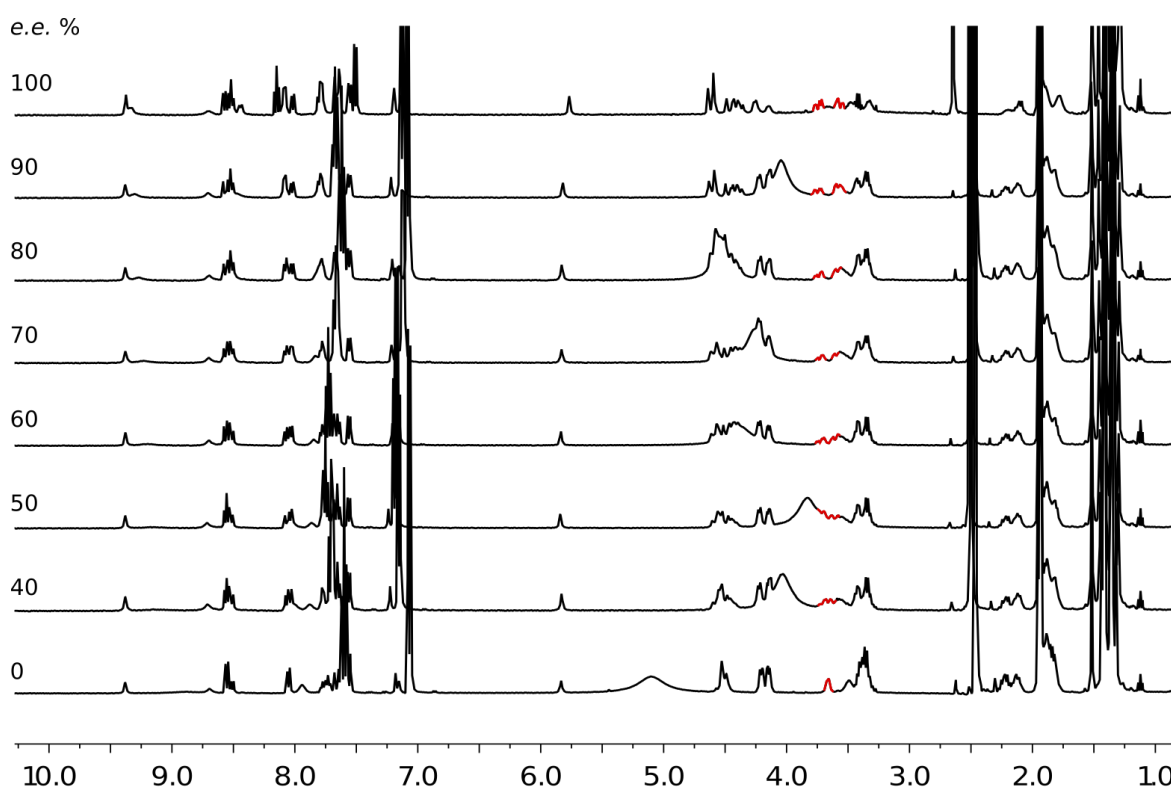
Figure S9: Stacked spectra showing changes at the GlyNH$_2$ probe with changes in *e.e.* of binding BocPro in CD$_3$CN (400 MHz, 298 K). GlyNH$_2$ reporter highlighted in red.

7.6 Variable temperature NMR (VT-NMR) studies of complexed Zn(1).2ClO$_4$

It was hoped that VT-NMR would clarify the mechanism by which Zn(**1**).2ClO$_4$ can sense *e.e.*, for example by the exchange of bound carboxylates. Several dynamic processes are proposed to occur in Zn(**1**).2ClO$_4$ (see Figure S10). The Aib tetramer body exists as two rapidly interconverting *M* and *P* 3$_{10}$-helices at room temperature (Figure S10c), with Solà and co-workers reporting that these interconverting helices can undergo slow exchange at 213K in CD$_3$OD.[12]

(a)
- Interconversion between the Λ and Δ propeller twists
- Zhang and co-workers reported rapid exchange of the propeller conformations of an isomorphous [Cu(MeTQA)(NCS)]$^{2+}$ at 0 °C in CD$_2$Cl$_2$

(b)
- BocProline has two rotameric forms: *cis* and *trans*
- Coalescence at 321 K
- On increasing T, switch from *trans* to *cis*

(e)
- D/L BocPro exchange at the Zn^{II}-metal centre must be fast to see averaging in the ^{1}H NMR spectrum

(d)
- Inversion at the central N of the BQPA ligand.
- Liang and co-workers reported the inversion of isomers with different N-configuration in a Zn^{II}-metal complex
- Fast inversion at 155 °C in DMSO-*d$_6$*
- Slow inversion at 25 °C in DMSO-*d$_6$*

(c)
- *M* ⇌ *P* conformers are under fast exchange at 298 K
- Exhibit coalescence at approx. 243 K
- Slow exchange of Aib conformers has been identified with a C-terminal Aib** reporter (213 K)

Figure S10: Possible conformational dynamics of Zn(**1**).2ClO$_4$ with BocPro bound.

BocPro has two rotamers, *cis* and *trans,* due to restricted rotation around the C-N bond of the carbamate (Figure S10b). The *cis*-rotamer of *N*-carbamylated amino acids are generally more stable due to the formation of intermolecular hydrogen-bonding species.[13,14] BocPro has a low interconversion barrier of about 20 kcal.mol^{-1} and fast/intermediate/slow rotation around this bond may also be evident.[15,16]

Furthermore, at the [Zn^{II}(BQPA)] binding site both the propeller conformation and complexation of the chiral carboxylate could undergo dynamic processes (Figure S10a,e). Zhang and co-workers investigated the conformational dynamics of Cu^{II} propeller complexes of tripodal ligands such as [Cu^{II}(MeTQA)] (Figure S10a),[17] and showed that exchange of Λ (left-handed) and Δ (right-handed) propeller conformations was fast even at low temperatures (−20 °C), suggesting that different propeller twists of Zn(**1**).2ClO$_4$ may be difficult to observe. Furthermore, exchange between coordinated quinolyl arms is possible (Figure S10d). Liang demonstrated this concept using VT-NMR spectroscopy on diastereoisomeric Zn^{II} complexes with two different aryl 'arms'. However, exchange between the arms was slow at room temperature, only becoming rapid at >100 °C.[18] Indeed the methylene protons of the quinolyl arms in Zn(**1**).2ClO$_4$ are diastereotopic at 298 K. Finally, exchange between the Zn(II)-metal centre and BocPro (D and L) may be fast on the NMR timescale as averaged peaks for Zn(**1**).2ClO$_4$ are observed in the ^{1}H NMR spectrum upon mixing with scalemic mixtures of BocPro (Figure S10e).

7.6.1 VT-NMR spectra of Zn(1).2ClO$_4$ (either Boc-D-Pro or *rac*-BocPro bound) in CD$_3$CN

VT-NMR spectra of Zn(**1**).2ClO$_4$ (Boc-L-Pro bound) and Zn(**1**).2ClO$_4$ (*rac*-BocPro) were obtained in CD$_3$CN over the temperature range of 40 °C to −40 °C (Figures S11 and S12 respectively). As expected, the *cis* and *trans* rotameric forms of the coordinated Boc-Pro were observed in both Boc-D-Pro bound and *rac*-BocPro bound Zn(**1**).2ClO$_4$. The *trans*-rotamer was favourable at low temperature whilst on increasing temperature the *cis*-rotamer became predominant, demonstrated at the α-proton of BocPro (resonances between 4.0 and 4.25 ppm in Figure S11). Slower interchange between the *M* and *P* helical conformations of the Aib foldamer were also observed upon a decrease in temperature. Line broadening of the ABX-system for Zn(**1**).2ClO$_4$ (Boc-D-Pro bound) ascribed to the GlyNH$_2$ protons (resonances between 3.5 and 3.7 ppm in Figure S11) and the Aib CH$_3$ protons (resonances between 1.1 and 1.7 ppm in Figure S11) were observed. Similarly, for Zn(**1**).2ClO$_4$ (*rac*-BocPro bound), line broadening was also observed for the doublet ascribed to the GlyNH$_2$ (resonances between 3.5 and 3.7 ppm in Figure S12). Unfortunately, decoalescence of the NMR signals was not reached within the temperature range suitable for CD$_3$CN.
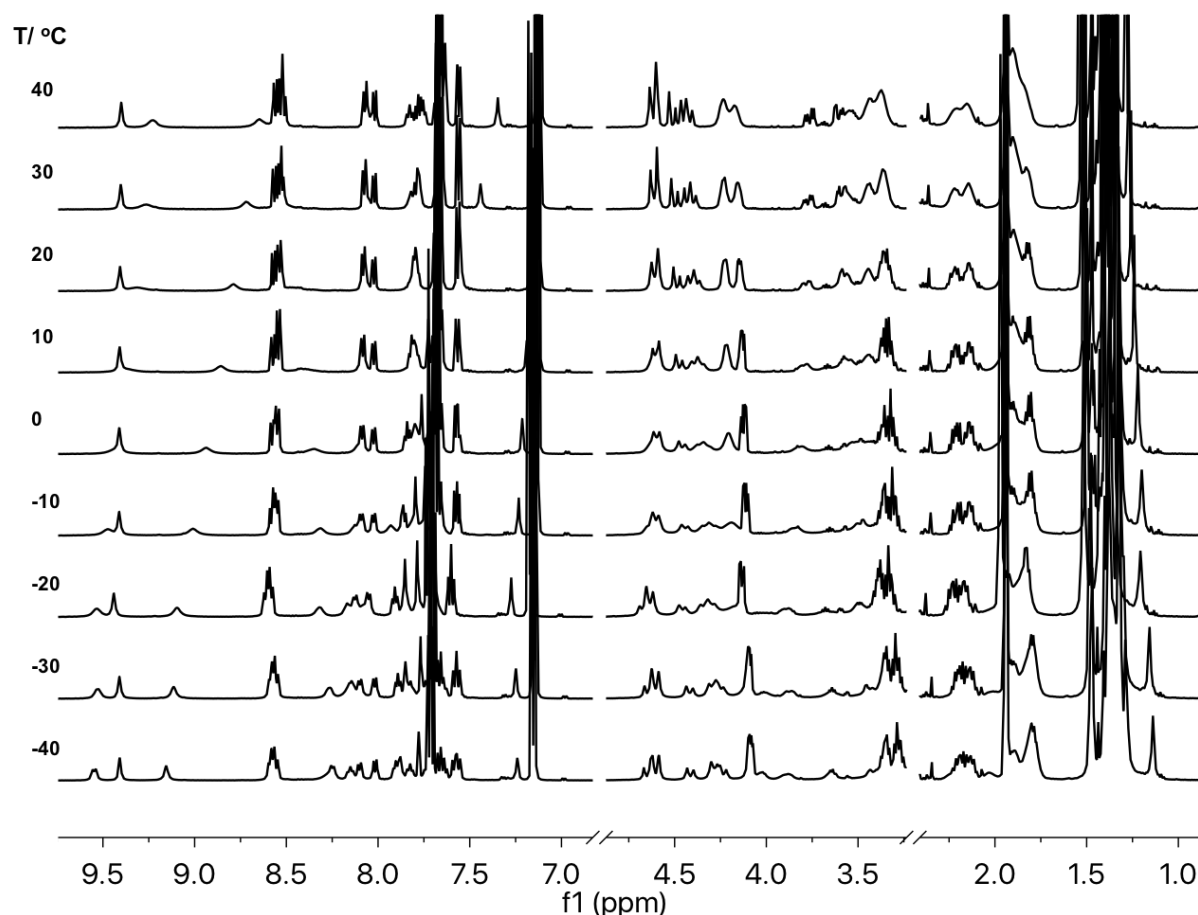
Figure S11: Variable temperature ^{1}H NMR spectra of Boc-D-Pro bound Zn(**1**).2ClO$_4$ (2 eq. of Boc-D-Pro, 2.4 eq. 2,6-lutidine) in increments of 10 °C (CD$_3$CN, 400 MHz).

The aromatic and pyridyl methylene proton resonances of the [Zn^{II}(BQPA)] binding site displayed significant changes over the temperature range of 40 °C to −40 °C for both bound Boc-D-Pro and *rac*-BocPro. Firstly, from 40 to −10 °C, broadening of the quinolone Ar-H and quinoline methylene proton resonances were observed. This was most noticeable for the quinolyl and pyridyl methylene protons (resonances between 4.5 and 4.7 ppm in Figures S11 and S12). With a continued decrease in temperature from −10 °C to −40 °C, the signals began to sharpen again, although complete resolution of the signals was not reached. Despite this, the left- (Λ) and right-handed (Δ) propeller conformations appear to be still in fast exchange as only one set of signals were observed and there were no changes in anisochronicity. Chemical shifts were observed for the aromatic and methylene protons of the quinolyl arms at −40 °C and resolution was also increased with any overlapping peaks that correspond to non-equivalent quinoline arms. Interestingly, analogous spectra were obtained for Zn(**1**).2ClO$_4$ (Boc-L-Pro bound) and Zn(**1**).2ClO$_4$ (*rac*-BocPro bound) at −40 °C, despite their differences at higher temperatures.

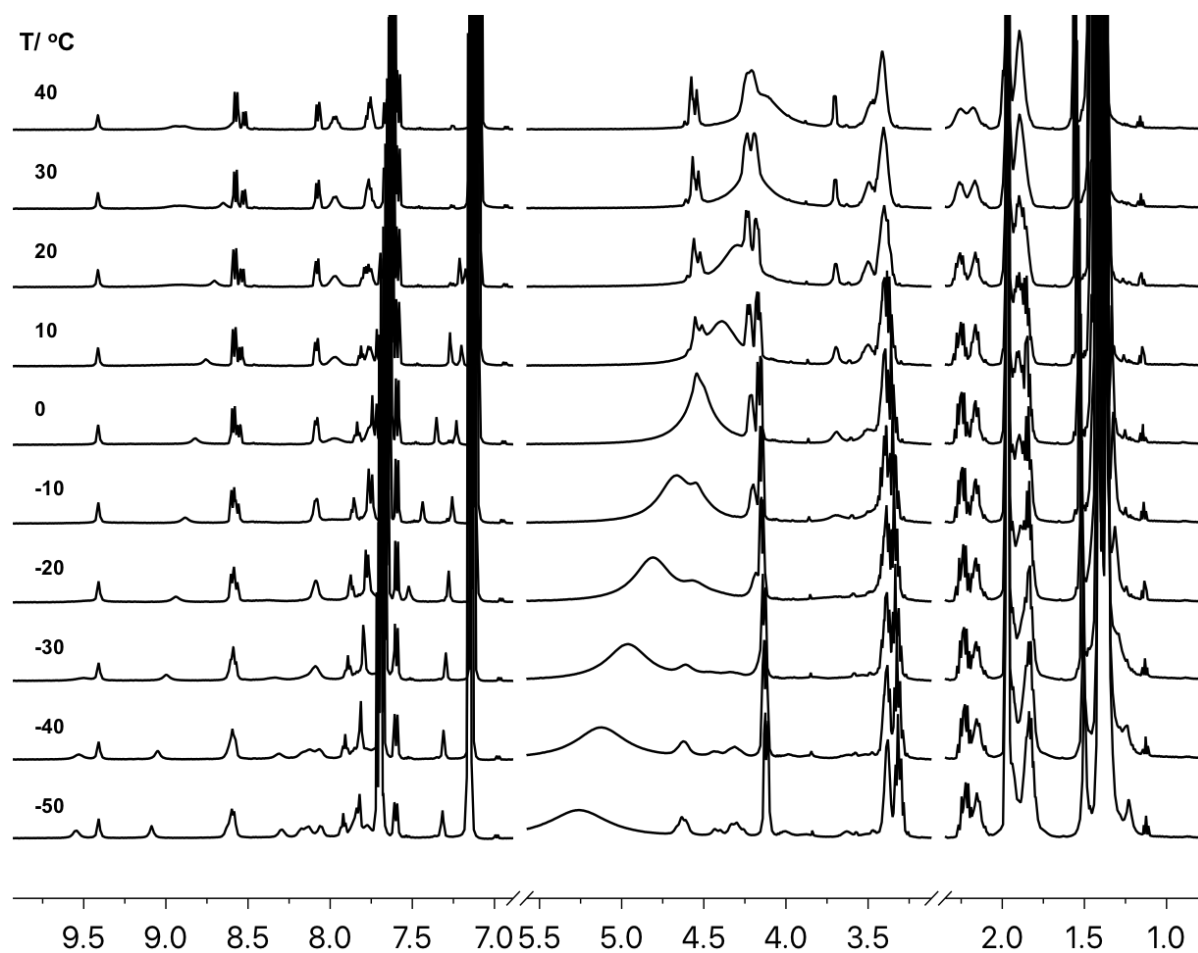**Figure S12:** Variable temperature ^{1}H NMR spectra of *rac*-BocPro bound Zn(**1**).2ClO$_4$ (2 eq. of *rac*-BocPro, 2.4 eq. 2,6-lutidine) in increments of 10 °C (CD$_3$CN, 400 MHz).

7.6.2 VT-NMR spectra of Zn(1).2ClO$_4$ (either Boc-D-Pro or rac-BocPro bound) in CD$_3$OD

As CD$_3$OD has proven to be a better solvent system for observing foldamer dynamics,[12] VT-NMR spectra of Zn(1).2ClO$_4$ (Boc-D-Pro bound) and Zn(1).2ClO$_4$ (rac-BocPro bound) were also acquired in CD$_3$OD over a temperature range of −50 °C to 40 °C. At 20 °C, several peaks in the mixture of Zn(1).2ClO$_4$ with Boc-D-Pro, including the GlyNH$_2$ methylene and quinolyl protons, were resolved (Figure S13) whereas the ^{1}H NMR spectrum of Zn(1).2ClO$_4$ with rac-BocPro was very broad (Figure S14). Due to the broadness observed for the mixture of Zn(1).2ClO$_4$ with rac-BocPro, and the GlyNH$_2$ being concealed by peaks from BocPro in this solvent, it is difficult to analyse these spectra fully.
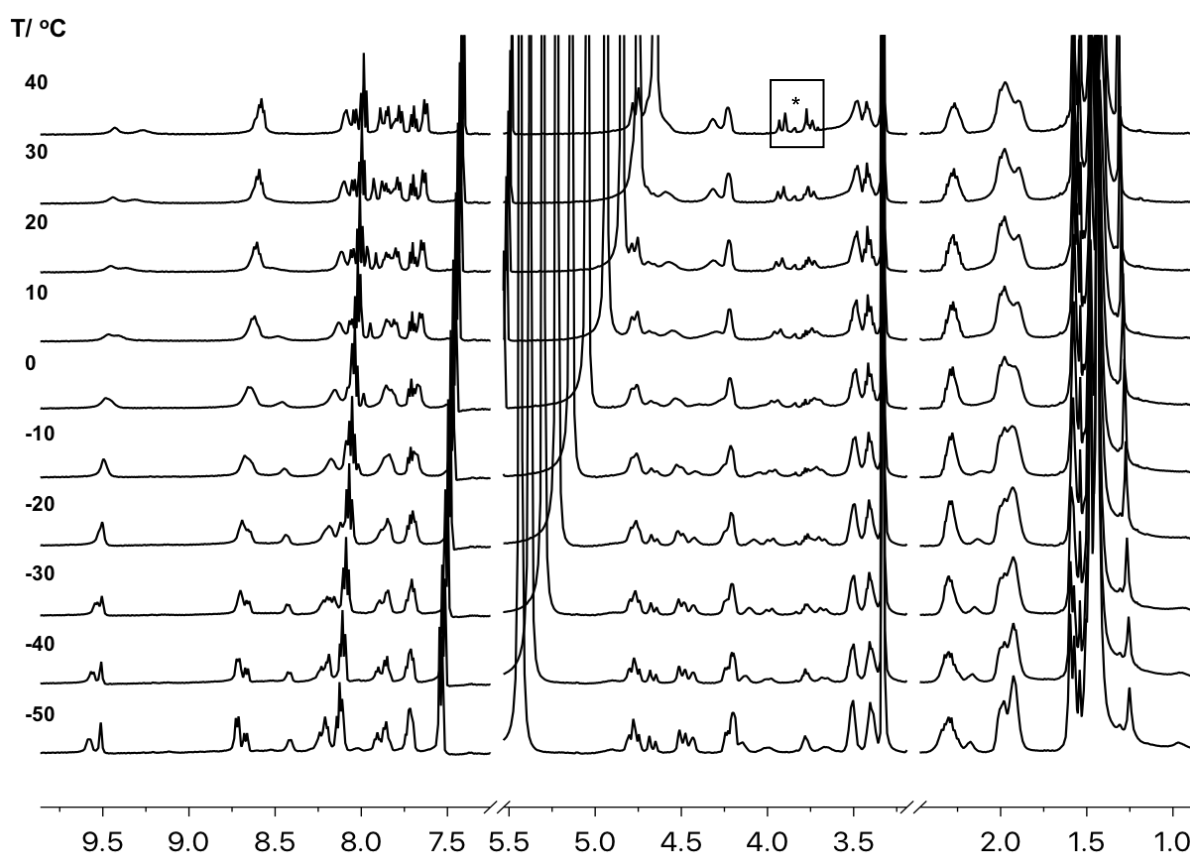

Figure S13: Variable temperature ^{1}H NMR spectra of Boc-D-Pro bound Zn(1).2ClO$_4$ (2 eq. of Boc-D-Pro, 2.4 eq. 2,6-lutidine) in increments of 10 °C (CD$_3$OD, 400 MHz). * Indicates methylene of GlyNH$_2$.

Upon decreasing the temperature, slower interchange of the *M* and *P* Aib helical conformations were observed for the mixtures of Zn(1).2ClO$_4$ with rac-BocPro and with Boc-D-Pro, suggested by the broadening of the Aib and GlyNH$_2$ methylene resonances (latter resonances between 3.6 and 4.0 ppm in Figure S13 and S14). No splitting of the GlyNH$_2$ methylene resonances was observed in the mixture of Zn(1).2ClO$_4$ with rac-BocPro; any splitting might have suggested ligand exchange at the metal had become slow. However, for

the aromatic protons and quinolyl methylene protons of the [Zn^{II}(BPQA)] binding site, changes in chemical shifts were observed, along with sharpening of all aromatic resonances. Only one set of resonances were observed suggesting that the propeller conformations are in fast exchange.
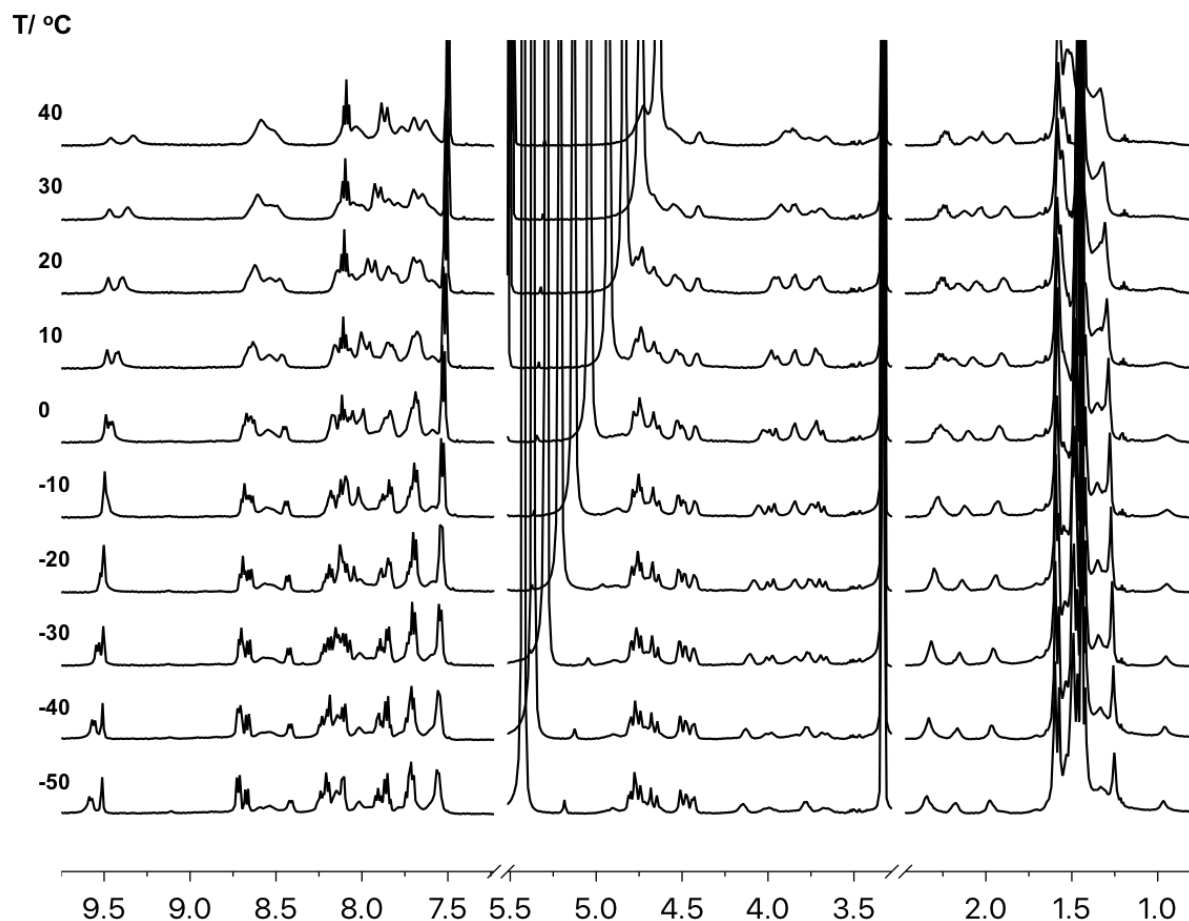
Figure S14: Variable temperature ^{1}H NMR spectra of *rac*-BocPro bound Zn(**1**).2ClO$_4$ (2 eq. of *rac*-BocPro, 2.4 eq. 2,6-lutidine) in increments of 10 °C (CD$_3$OD, 400 MHz, 298 K).

In neither solvent was splitting of the GlyNH$_2$ methylene resonances observed in the mixture of Zn(**1**).2ClO$_4$ with *rac*-BocPro, although such changes may have been obscured by broadening caused by gradual decoalescence of key resonances.

7.7 Titration of Zn(1).2ClO$_4$ with the monoester 3a, 3b, 3c, 3d or 3e (with 2,6-lutidine) in CD$_3$CN

A stock solution of the required monoester was made by dissolving the monoester (75 µmol) and 2,6-lutidine (90 µmol) in CD$_3$CN (1 mL). A stock solution of the host (15 mM) was made up by dissolving Zn(**1**).2ClO$_4$ (75 µmol) in CD$_3$CN (5 mL). An aliquot of the host stock solution was added to a NMR tube (500 µL, 7.5 µmol) and a NMR spectrum was acquired for reference. For monitoring the binding of the monoester to Zn(**1**).2ClO$_4$, aliquots of the monoester solution (100 µL = 1 eq. acid, 1.2 eq. base) were sequentially added and a spectrum was acquired after each addition until 22.5 µmol of carboxylate and 27.0 µmol of 2,6-lutidine were added. Anisochronicity was recorded at the GlyNH$_2$ probe (δ_{gly} = 3.6 ppm).
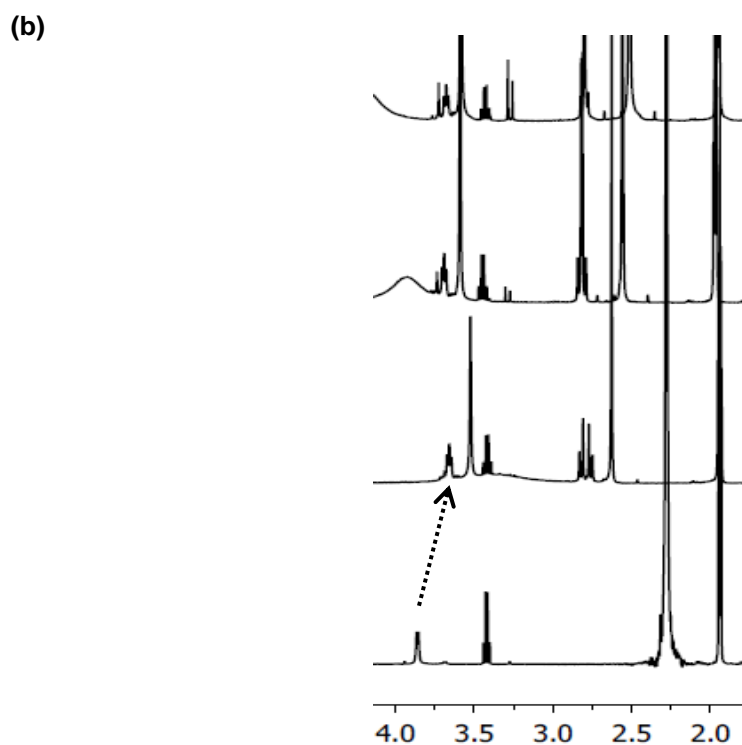
(a)

(b)
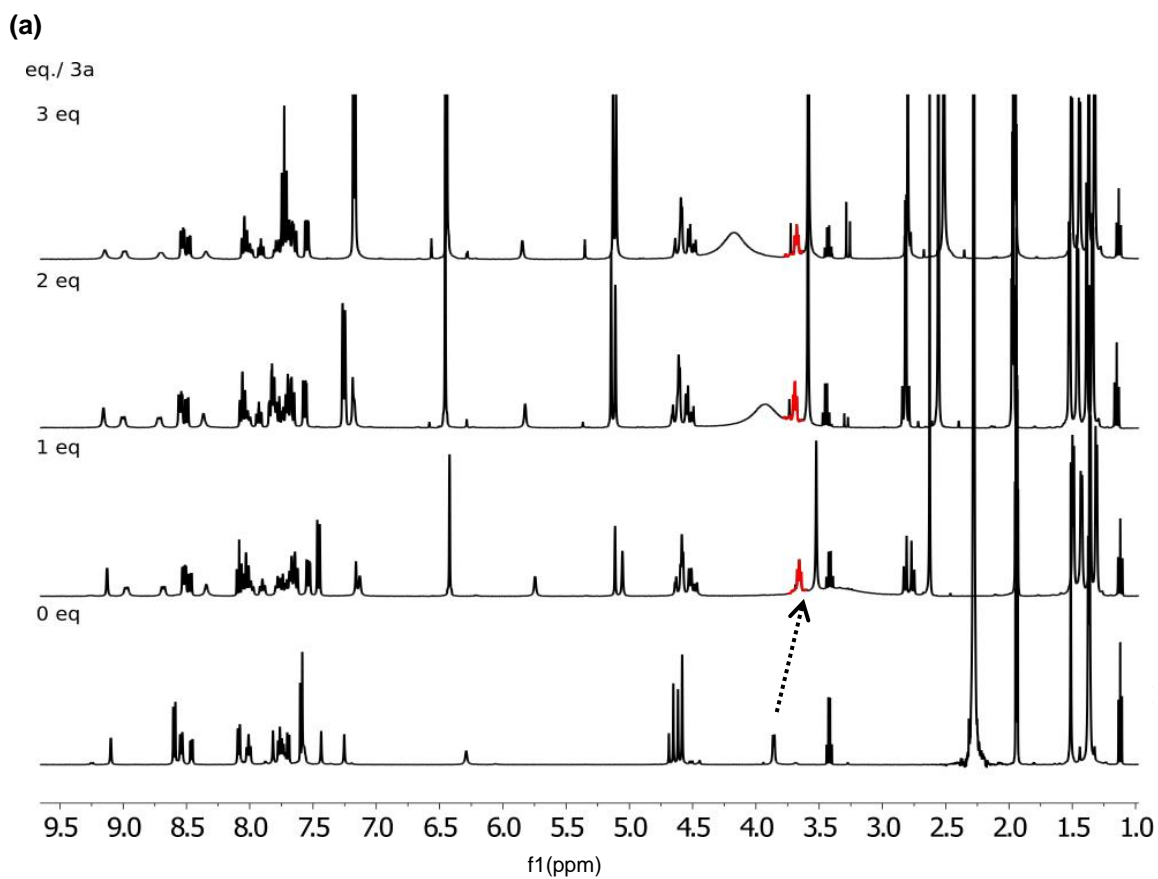
Figure S15: (a) ^{1}H NMR spectrum of Zn(**1**).2ClO$_4$ with **3a** (0–3 eq.) and 2,6-lutidine (0–3.6 eq.) in CD$_3$CN (400 MHz, 298 K). GlyNH$_2$ reporter highlighted in red. **(b)** Expansion of GlyNH$_2$ region.

(a)

eq./ 3b

3 eq

2 eq

1 eq

0 eq

f1 (ppm)
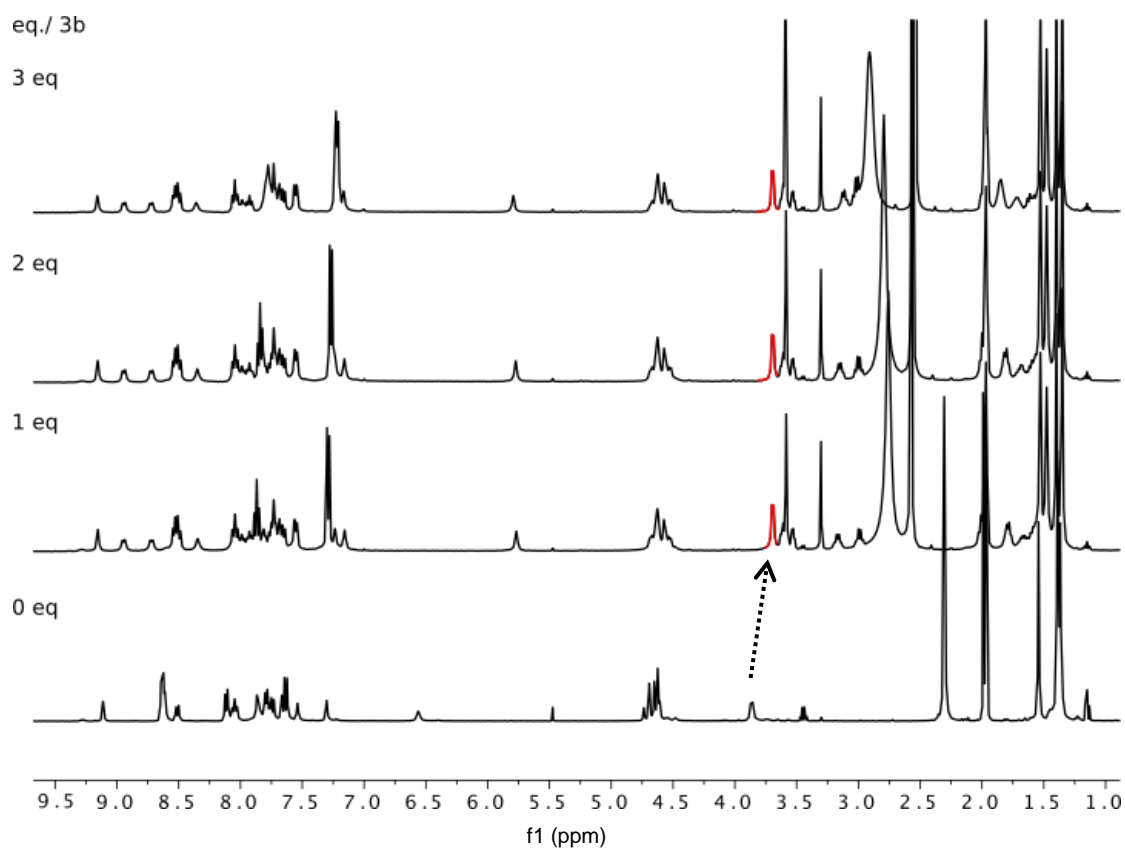
(b)
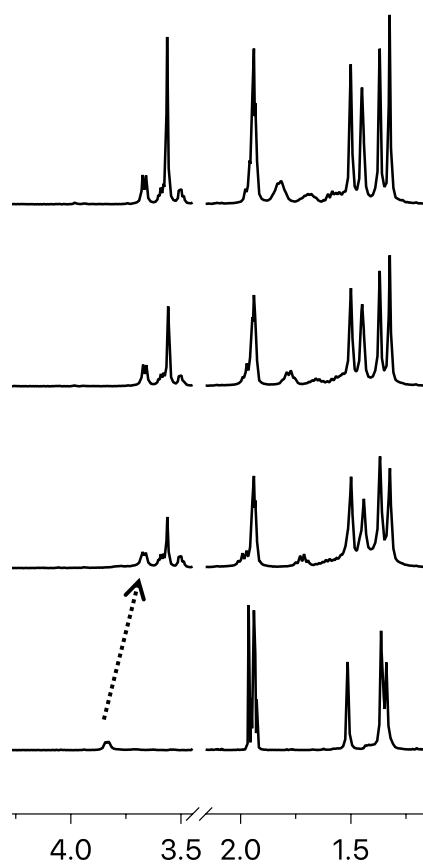
Figure S16: (a) ^{1}H NMR spectrum of Zn(**1**).2ClO$_4$ with **3b** (0–3 eq.) and 2,6-lutidine (0–3.6 eq.) in CD$_3$CN (400 MHz, 298 K). GlyNH$_2$ reporter highlighted in red. **(b)** Expansion of GlyNH$_2$ and Aib region.
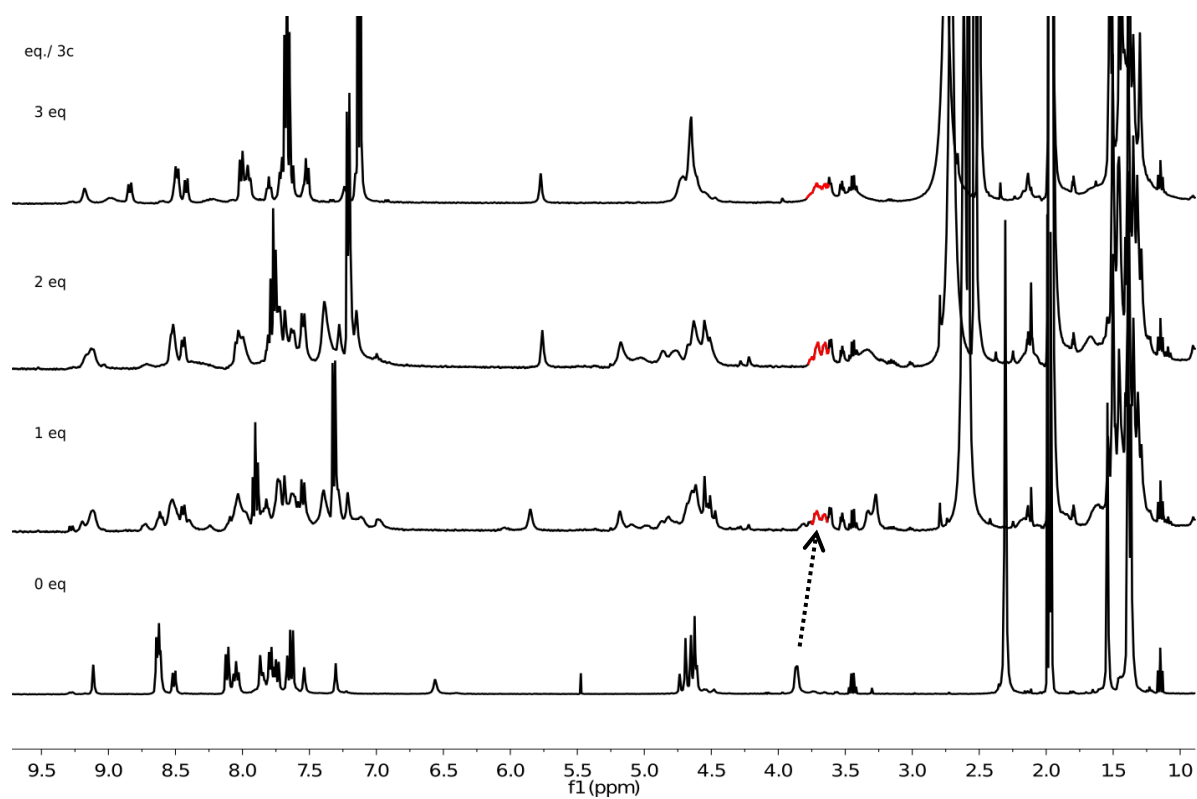
Figure S17: ^{1}H NMR spectrum of Zn(**1**).2ClO$_4$ with **3c** (0-3 eq.) and 2,6-lutidine (0-3.6 eq.) in CD$_3$CN (400 MHz, 298 K). GlyNH$_2$ reporter highlighted in red.
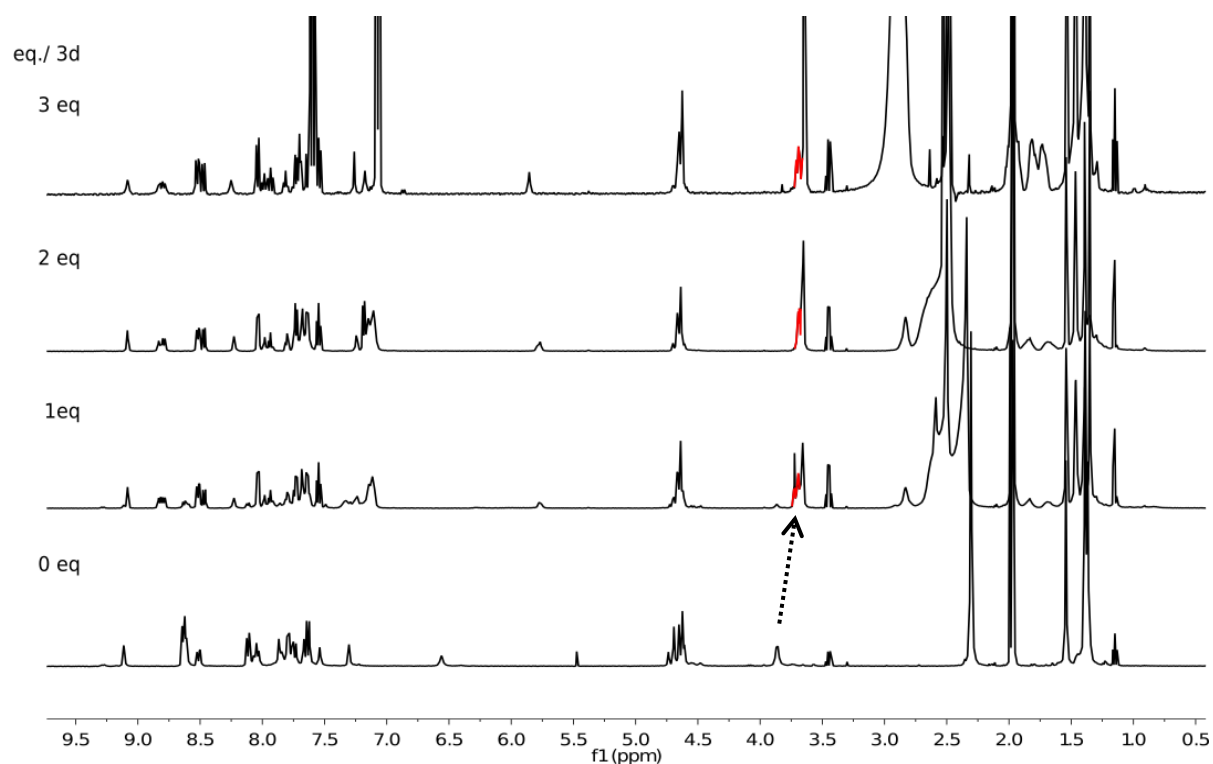
Figure S18: ^{1}H NMR spectrum of Zn(**1**).2ClO$_4$ with **3d** (0–3 eq.) and 2,6-lutidine (0–3.6 eq.) in CD$_3$CN (400 MHz, 298 K). GlyNH$_2$ reporter highlighted in red.
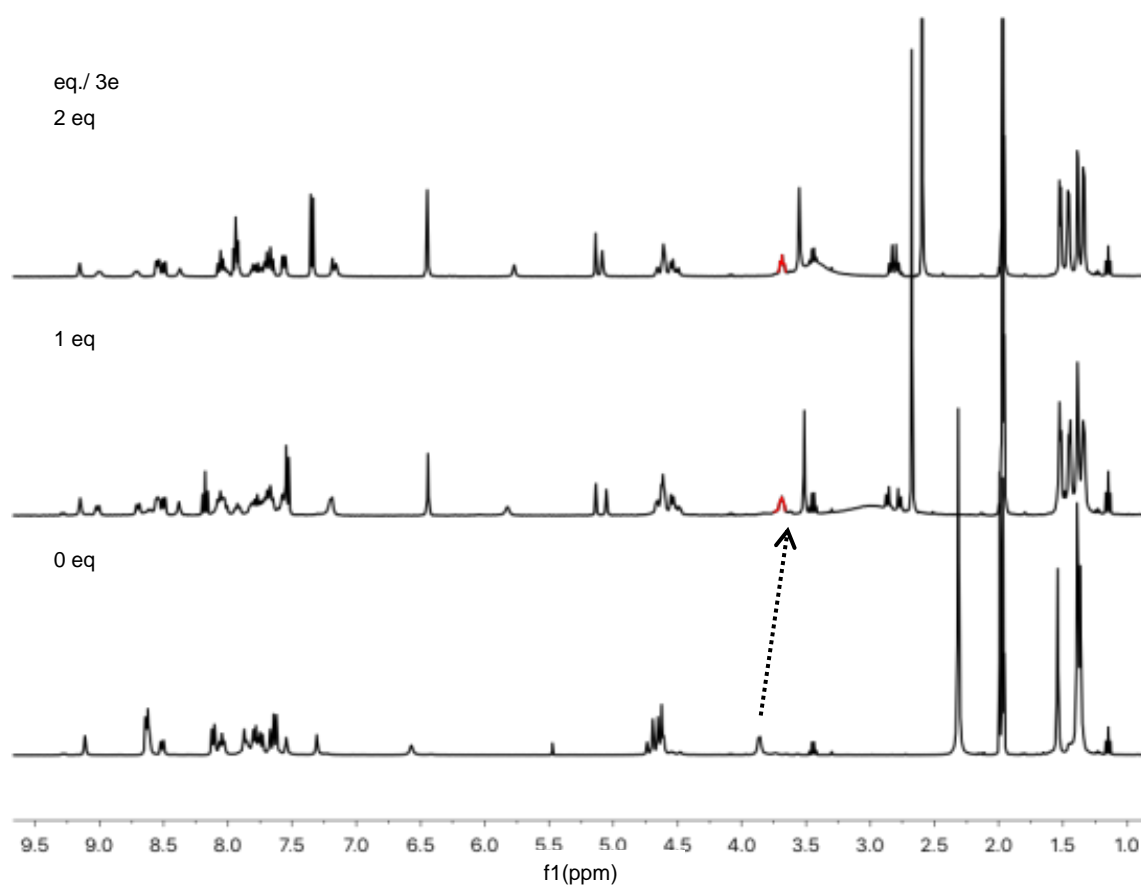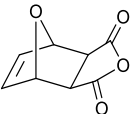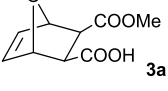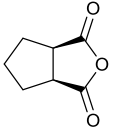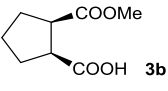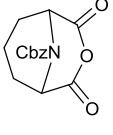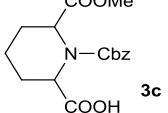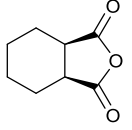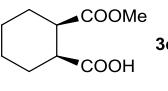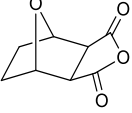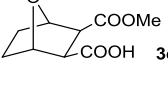
Figure S19: ^{1}H NMR spectrum of Zn(**1**).2ClO$_4$ with **3e** (0–3 eq.) and 2,6-lutidine (0–3.6 eq.) in CD$_3$CN (400 MHz, 298 K). GlyNH$_2$ reporter highlighted in red.

7.8 Splitting of GlyNH$_2$ methylene induced by a variety of monoester products from methanolytic desymmetrisation of *meso*-anhydrides catalysed by 4.

Table S3: Methanolytic desymmetrisation conditions for a variety of *meso*-anhydrides with catalyst **4** in anhydrous THF.

Entry	Anhydride	Product	*T, t* / °C, h	4, MeOH / equiv.	Yield / %	*e.e.* / %
1	2a	COOMe COOH 3a	25, 24	0.1, 10	98%	92[a]
2	2b	COOMe COOH 3b	25, 48	0.1, 10	>98%	94[a]
3	CbzN 2c	COOMe N—Cbz COOH 3c	-20, 7	1.1, 1	90%	93[a]
4	2d	COOMe COOH 3d	25, 48	0.1, 10	>98%	~100[b]
5	2e	COOMe COOH 3e	25, 26	0.1, 10	98%	91[b]

[a] *e.e.* determined by chiral HPLC. [b] *e.e.* determined by ^{1}H NMR spectroscopy.
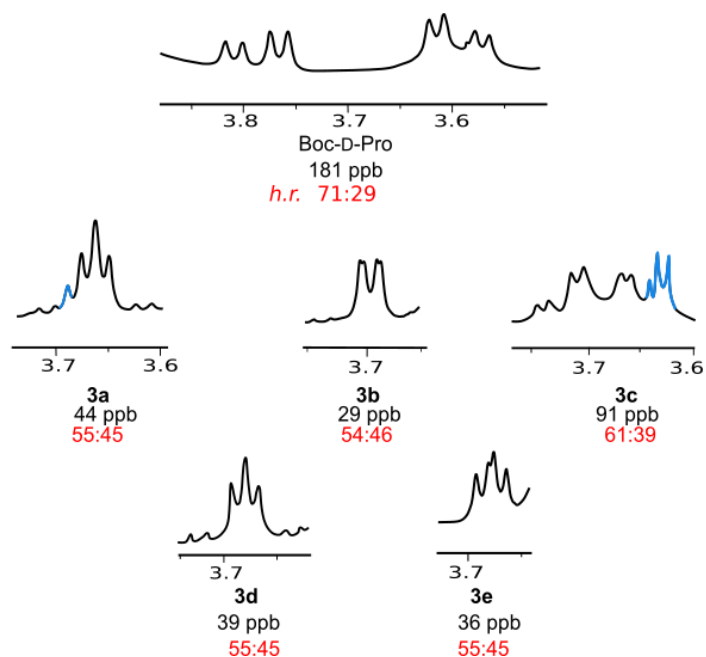
Figure S20: Partial ^{1}H NMR spectra in CD$_3$CN showing the signals of the methylene in the GlyNH$_2$ reporter of Zn(**1**).2ClO$_4$ bound to carboxylates **3a-3e.** Impurities are highlighted in blue.

Table S4: Measured *e.e.*, observed GlyNH$_2$ methylene anisochronicity and calculated screw-sense induction of a series of chiral carboxylate ligands that bind Zn(**1**).2ClO$_4$.

Entry	Anhydride	Carboxylate	*e.e.* / %	$\Delta\delta^a$ / ppb	*h.e.*$_o^b$ / %	*h.r.*$_o$
1	**2a**	**3a**	92	44	10	55:45
2	**2b**	**3b**	94	29	7	54:46
3	**2c**	**3c**	93	110	31	64:36
4	**2d**	**3d**	~100	39	10	54:45
5	**2e**	**3e**	91	36	10	55:45

^{a} Chemical shift separation of GlyCH$_2$ peaks at 25 °C in CD$_3$CN. ^{b} Calculated using $\Delta\delta_{slow}$ = 630 ppb in CD$_3$CN and p = 0.947.[12]

8. CD spectroscopy studies of Zn(1).2ClO$_4$

8.1 CD spectroscopy experimental details

Circular Dichroism (CD) measurements were performed at 20 °C on a Chirascan[TM] spectrometer (light source: 150 W xenon) or on a JASCO J-815 spectropolarimeter, using a 1 mm cell with the solvent and concentration stated, where applicable. HPLC grade MeCN was used.

8.2 Determination of binding strength: CD titration of Zn(1).2ClO$_4$ with Boc-L-Pro, 2,6 lutidine in MeCN

A stock solution of Zn(**1**).2ClO$_4$ was made up by dissolving 0.0125 mmol in 10 mL of MeCN. A stock solution of the chiral carboxylic acid (e.g. Boc-Xaa-OH) was prepared by dissolving guest (0.0125 mmol) and 2,6-lutidine (1.2. eq., 0.0150 mmol) in acetonitrile (10 mL). Each point on the titration was a separate solution, containing 0.2 mL of the host solution and 0–0.8 mL of the guest and the total volume diluted to 1 mL with solvent such that [Zn(**1**).2ClO$_4$] = 0.25 mM and [carboxylic acid] = 0–1 mM.

(a)

(b)

Acid	K / M^{-1}
Boc-Ala	8.0 x 10^5
Boc-Phe	1.5 x 10^5
Boc-Val	1.5 x 10^6
Boc-αMv	7.1 x 10^5
Boc-Pip	8.6 x 10^5
Boc-Pro	2.2 x 10^5
Boc-Ser	2.8 x 10^6
Boc-Gln	3.2 x 10^5
Boc-Glu	4.6 x 10^5
(S)-ketopinic acid	1.7 x 10^6
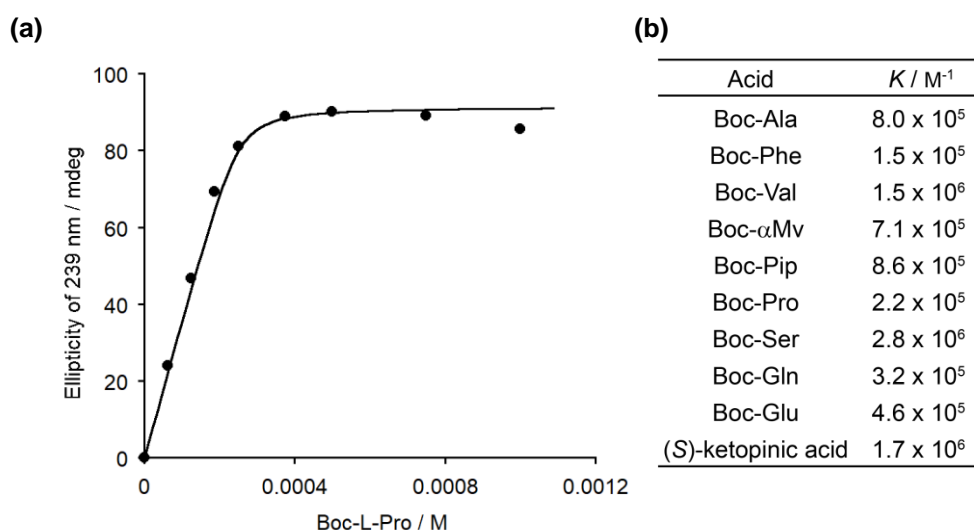
Figure S21: (a) Change in the CD signal at 239 nm with increasing concentration of Boc-L-Pro (0-1 mM) in Zn(**1**).2ClO$_4$ (0.25 mM) in MeCN. Fit is shown for 1:1 binding with K = 2.2 × 10^5 M^{-1}. Binding constant (K) value determined by Dynafit.[19] **(b)** Binding constants determined by Dynafit for analogous titrations of Zn(**1**).2ClO$_4$ (0.25 mM) with other carboxylic acids.

A titration plot of the ECCD response at 239 nm (Figure S21) can be used to determine binding constants. Dynafit[19] was used to perform nonlinear least-squares regression analysis of the titration data for a range of the chiral acids. All the determined K values were within an order of magnitude of one another, between 10^5 and 10^6 M^{-1}. However, the difference in appearance of the titration plots between the strongest and weakest binders was small.
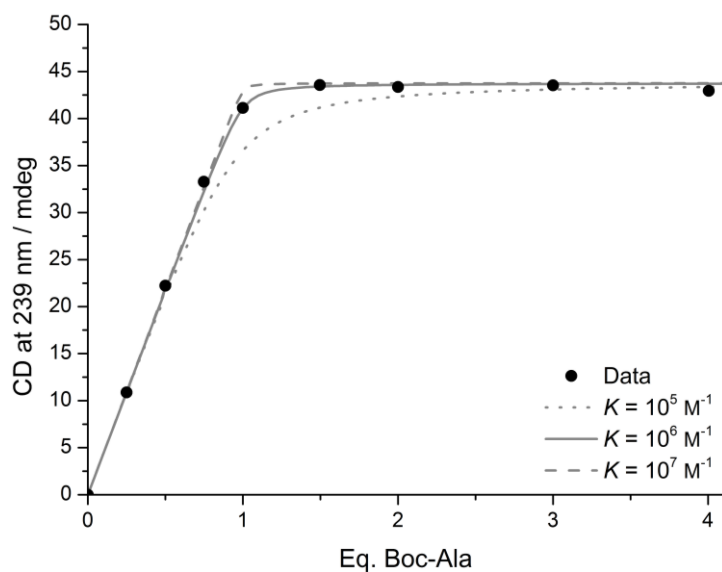
Figure S22: Titration curve (points) for Zn(**1**).2ClO$_4$ (0.25 mM) in MeCN with increasing concentration of Boc-Ala (0-1 mM) and lutidine (0-1.2 mM); nonlinear least-squares regression fits where $K = 10^5$, 10^6 and 10^7 M^{-1}.

Figure S22 shows the experimental data for the titration of Boc-Ala into Zn(**1**).2ClO$_4$ with calculated titration curves shown for $K = 10^5$, 10^6 and 10^7 M^{-1}. The binding interaction is too strong to be fitted accurately in this way, as the concentration of Zn(**1**).2ClO$_4$ required to produce a good CD signal (2.5 × 10^{-4} M) is too high for determining K. Nonetheless, these CD titrations provided $K > 10^5$ M^{-1} in all measured cases.

8.3 Determination of ECCD on *e.e.*: CD titration of Zn(1).2ClO$_4$ with scalemic mixtures of BocPro and 2,6 lutidine in MeCN

The appropriate scalemic mixture of Boc-L-Pro and Boc-D-Pro (L/D ratio = 0:100, 40:60, 50:50, 60:40, 70:30, 80:20, 90:10, 100:0, [Boc-L-Pro] + [Boc-D-Pro] = 0.5 mM) was added to a solution of Zn(**1**).2ClO$_4$ (0.25 mM) and 2,6-lutidine (0.60 mM) in acetonitrile. All values refer to final concentrations in the cuvette, within a volume of 300 µL solvent. Each point on the titration was a separate solution containing a different scalemic mixture.

8.4 Titration of Zn(1).2ClO$_4$ with 3b (*e.e.* = 95%)
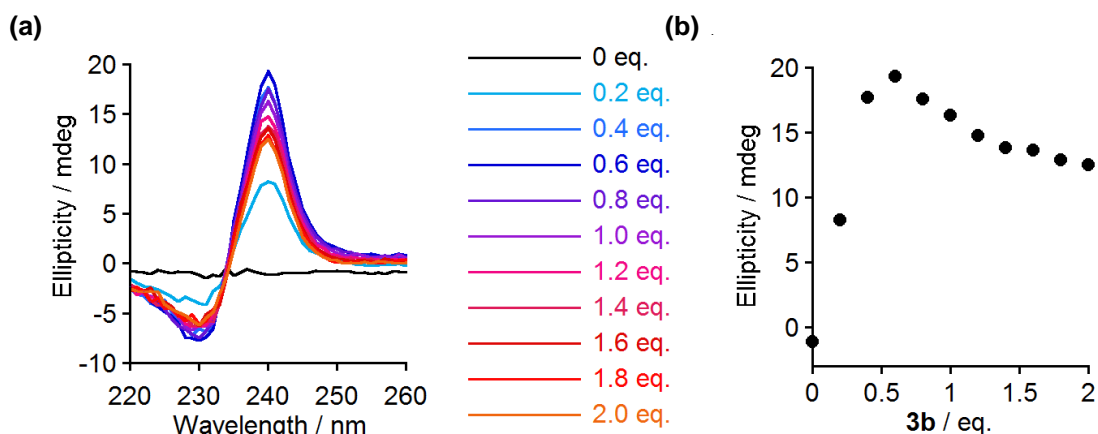
Figure S23: (a) CD spectra of Zn(**1**).2ClO$_4$ (0.25 mM) in MeCN titrated with **3b** (0 to 2 eq.) and 2,6-lutidine (2.4 eq.). (b) Change in the CD signal at 239 nm upon titration of Zn(**1**).2ClO$_4$ (0.25 mM) with **3b** (0 to 2 eq.) and 2,6-lutidine (2.4 eq.) in MeCN.

8.5 Addition of 3b (*e.e.* = 0 %) to Zn(1).2ClO$_4$
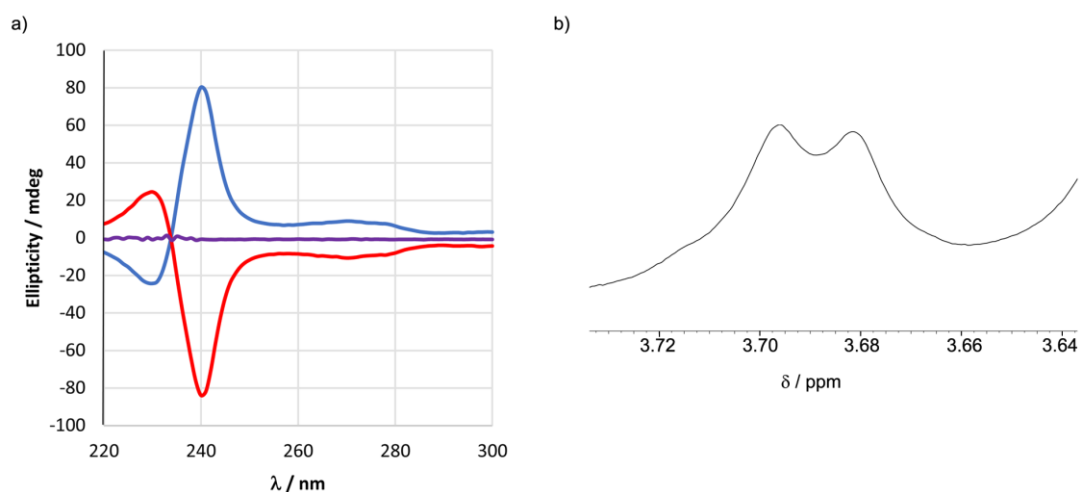
Figure S24: (a) CD spectra of Zn(**1**).2ClO$_4$ (0.25 mM) with racemic **3b** (2 eq. in CD$_3$CN, purple), Boc-L-Pro (2 eq. in MeCN, blue), Boc-D-Pro (2 eq. in MeCN, red) and 2,6-lutidine (2.4 eq.). (b) Expansion of the ^{1}H NMR spectrum of Zn(**1**).2ClO$_4$ (6.8 mM) in CD$_3$CN with racemic **3b** and 2,6-lutidine (2.4 eq.), showing an apparently isochronous signal split only by the adjacent NH.

9. Fluorescence spectroscopy studies of Zn(1).2ClO$_4$

Fluorescence spectroscopy was carried out on a Varian Cary Eclipse fluorimeter, using a 10 mm cell at the stated concentration. HPLC grade MeCN was used.

9.1 Determination of binding strength: Fluorescence titration of Zn(1).2ClO$_4$ with Boc-L-Pro, 2,6 lutidine in MeCN

Complex Zn(**1**).2ClO$_4$ was found to be fluorescent, and upon excitation at 280 nm it fluoresces with λ_{em} = 381 nm in acetonitrile. Quinoline-based tripodal ligands form the basis of a range of fluorescent-based Zn sensors,[20] and binding of a carboxylate can quench this emission, presumably by electron transfer from the carboxylate (donor) to the excited quinolines of the BQPA (acceptor).[21] The concentration of Zn(**1**).2ClO$_4$ required to get an emission signal strong enough to detect was 1.25×10^{-5} M^{-1}, which is twenty times more dilute than the concentration used for the CD titration and should give more accurate values for the affinity of carboxylates for the Zn centre in Zn(**1**).2ClO$_4$. Just 1 eq. lutidine was used to form the carboxylate *in situ* as it was also found to quench fluorescence emission through binding to the remaining solvent-bound complex. Binding constants were determined by fluorescence quenching titrations for Boc-L-Ala, Boc-L-Pip, Boc-Aib and Boc-L-Pro (e.g. Figure S25), with a minimum of three repeats for each acid. Fitting of the data using Dynafit[19] gave K values around 3×10^6 M^{-1} for all these carboxylates, which agree with the range determined by CD titrations (Section 8.1). Mean values and standard errors are shown (Table S5).
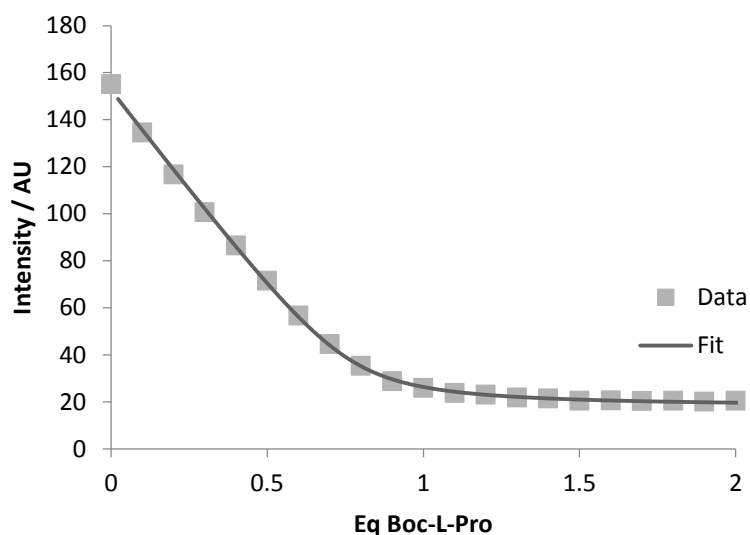
Figure S25: Titration curve (points) from fluorescence emission spectra (λ_{ex} = 280 nm) of Zn(**1**).2ClO$_4$ (12.5 µM) in MeCN with increasing concentration of Boc-L-Pro (0 to 25 µM) and lutidine (0 to 25 µM) and nonlinear least-squares regression fit (line); Fit for $K = (4.2 \pm 0.6) \times 10^6$ M^{-1} shown, as determined by Dynafit.[19]

Table S5: Fitted binding constants of Zn(1).2ClO$_4$ in MeCN for Boc-L-Pro, Boc-L-Pip, Boc-L-Ala and Boc-Aib

Carboxylic acid	Fitted binding constant / M^{-1}
Boc-L-Pro ($n = 4$)	$(4.2 \pm 0.2) \times 10^6$
Boc-L-Pip ($n = 3$)	$(2.3 \pm 0.2) \times 10^6$
Boc-L-Ala ($n = 3$)	$(2.8 \pm 0.2) \times 10^6$
Boc-Aib ($n = 3$)	$(3.9 \pm 0.2) \times 10^6$

10. Crystal data and refinement for Zn(1).2ClO₄
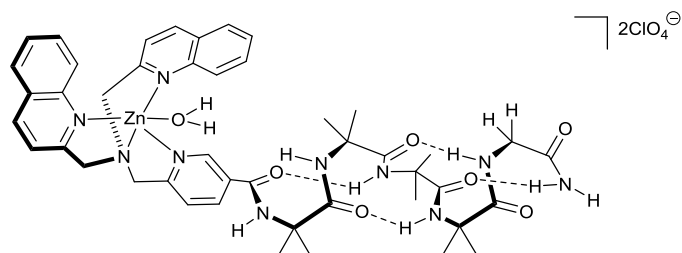
Data Collection: Single crystals for X-ray diffraction analysis were grown by the slow diffusion of Et₂O into a MeOH solution. Data were collected on a Rigaku-Oxford diffraction FR-X rotating anode using Mo-Kα radiation at 150K.

Structure solution: X-ray diffraction data were processed with the CrisAlisPro suite of programs. Absorption correction was carried out using Abstract 3 software. Crystal solution and refinement were carried out using SHELX and Olex2 suit of programs.[20,21] All atoms were refined anisotropically. Hydrogen atoms were placed in theoretical positions. Disordered anions were modelled over two positions.

Table S6: Crystal data and structure refinement for Zn(1).2ClO₄

Identification code	**Zn(1).2ClO₄**
Empirical formula	$C_{45}H_{66}Cl_2N_{10}O_{20}Zn$
Formula weight	1203.34
Temperature/K	150.00(10)
Crystal system	Triclinic
Space group	P-1
a/Å	9.3605(3)
b/Å	15.3297(4)
c/Å	20.4443(6)
α/°	102.353(2)
β/°	96.569(2)
γ/°	100.991(2)
Volume/Å³	2776.06(14)
Z	2
$\rho_{calc}g/cm^3$	1.440
μ/mm^{-1}	0.621
F(000)	1260.0
Crystal size/mm³	0.2 × 0.1 × 0.03

Radiation	MoKα (λ = 0.71073)
2Θ range for data collection/°	4.134 to 60.058
Index ranges	$-12 \leq h \leq 11$, $-21 \leq k \leq 18$, $-26 \leq l \leq 28$
Reflections collected	49493
Independent reflections	13632 [R_{int} = 0.0407, R_{sigma} = 0.0510]
Data/restraints/parameters	13632/98/784
Goodness-of-fit on F^2	1.047
Final R indexes [I>=2σ (I)]	R_1 = 0.0575, wR_2 = 0.1229
Final R indexes [all data]	R_1 = 0.0818, wR_2 = 0.1316
Largest diff. peak/hole / e Å^{-3}	1.21/–0.51

11. References

(1)   F. G. A. Lister, B. A. F. Le Bailly, S. J. Webb and J. Clayden, *Nat. Chem.*, 2017, **9**, 420–425.

(2)   C. G. Oliva, A. M. S. Silva, D. I. S. P. Resende, F. A. A. Paz and J. A. S. Cavaleiro, *Eur. J. Org. Chem.*, 2010, **18**, 3449–3458.

(3)   S. H. Oh, H. S. Rho, J. W. Lee, J. E. Lee, S. H. Youk, J. Chin and C. E. Song, *Angew. Chem.*, 2008, **120**, 7990–7993.

(4)   S. Sharma, S. Panja, A. Bhattacharyya, P. S. Dhami, P. M. Gandhi and S. K. Ghosh, *Dalton Trans.*, 2016, **45**, 7737–7747.

(5)   E. J. T. Chrystal, L. Couper and David J. Robins, *Tetrahedron* 1995, **51**, 10241-10252.

(6)   H.-S. Chong, K. Garmestani, L. H. Bryant, Jr., D. E. Milenic, T. Overstreet, N. Birch, T. Le, E. D. Brady and M. W. Brechbiel, *J. Med. Chem.* 2006, **49**, 2055-2062.

(7)   (a) R. E. Babine, T. M. Bleckman, E. S. Littlefield, H. E. Parge, L. A. K. Pelletier, C. T. Lewis, J. V. French, M. Imbacuan, S. Katoh, J. H. Tatlock, R. E. Showalter and J. E. Villafranca, *Bioorg. Med. Chem. Lett.*, 1996, **6**, 385-390. (b) S. Katoh, H. Kawakami, H. Tada, M. A. Linton, V. Kalish, J. H. Tatlock and J. E. Villafranca, PCT Int. Appl., 2000, WO 2000004020 A1 20000127.

(8)   A. Peschiulli, Y. Gun'ku and S. J. Connon, *J. Org. Chem.*, 2008, **73**, 2454–2457.

(9)   C. Bolm, I. Schiffers, C. L. Dinter and A. Gerlach, *J. Org. Chem.*, 2000, **65**, 6984–6991.

(10)   H. S. Rho, S. H. Oh, J. W. Lee, J. Y. Lee, J. Chin and C. E. Song, *Chem. Commun.,* 2008, 1208–1210.

(11)   C. Christov, P. González-Bulnes, F. Malhaire, T. Karabencheva, C. Goudet, J.-P. Pin, A. Llebaria and J. Giraldo, *ChemMedChem*, 2011, **6**, 131–140.

(12)   J. Solà, G. A. Morris and J. Clayden, *J. Am. Chem. Soc.*, 2011, **133**, 3712–3715.

(13)   D. Mizrahi, H. E. Gottlieb, V. Marks and A. Nudelman, *J. Org. Chem.*, 1996, **61**, 8401–8406.

(14)   S. Wernisch, O. Trapp and W. Lindner, *Anal. Chim. Acta*, 2013, **795**, 88–98.

(15)   B. D. Smith, D. M. Goodenough-Lashua, C. J. E. D'Souza, K. J. Norton, L. M. Schmidt and J. C. Tung, *Tetrahedron Lett.*, 2004, **45**, 2747–2749.

(16)   V. Kubyshkin, P. Durkin and N. Budisa, *New J. Chem.*, 2016, **40**, 5209–5220.

(17)   J. Zhang, K. Siu, C. H. Lin and J. W. Canary, *New J. Chem.*, 2005, **29**, 1147–1151.

(18)   J. Liang and J. W. Canary, *Chirality*, 2011, **23**, 24–33.

(19)   P. Kuzmic, *Anal. Biochem.*, 1996, **237**, 260–273.

(20)   Z. Xu, J. Yoon, and D. R. Spring, *Chem. Soc. Rev.*, 2010, **39**, 1996–2006.

(21)   D. Curiel, E. J. Hayes, and P. D. Beer, Advanced Concepts in Fluorescence Sensing: Part A: Small Molecule Sensing, Springer, 2007.

(22)   G. M. Sheldrick, *Acta Crystallogr.* 2015, **C71**, 3-8.

(23)   O. V. Dolomanov, L. J. Bourhis, R. J. Gildea, J. A. K. Howard and H. Puschmann, *J. Appl. Cryst.* 2009, **42**, 339–341